

Alma Mater Studiorum Università di Bologna
Archivio istituzionale della ricerca

Validating far-field deformation styles from the Adjara-Trialeti fold-and-thrust belt to the Greater Caucasus (Georgia) through multi-proxy thermal maturity datasets

This is the final peer-reviewed author's accepted manuscript (postprint) of the following publication:

Published Version:

Sveva Corrado, T.G. (2021). Validating far-field deformation styles from the Adjara-Trialeti fold-and-thrust belt to the Greater Caucasus (Georgia) through multi-proxy thermal maturity datasets. MARINE AND PETROLEUM GEOLOGY, 130, 1-18 [10.1016/j.marpetgeo.2021.105141].

Availability:

This version is available at: <https://hdl.handle.net/11585/821052> since: 2021-05-28

Published:

DOI: <http://doi.org/10.1016/j.marpetgeo.2021.105141>

Terms of use:

Some rights reserved. The terms and conditions for the reuse of this version of the manuscript are specified in the publishing policy. For all terms of use and more information see the publisher's website.

This item was downloaded from IRIS Università di Bologna (<https://cris.unibo.it/>).
When citing, please refer to the published version.

(Article begins on next page)

This is the final peer-reviewed accepted manuscript of:

Sveva Corrado, Thomas Gusmeo, Andrea Schito, Victor Alania, Onise Enukidze, Enrico Conventi, William Cavazza: *Validating far-field deformation styles from the Adjara-Trialeti fold-and-thrust belt to the Greater Caucasus (Georgia) through multi-proxy thermal maturity datasets*

MARINE AND PETROLEUM GEOLOGY vol. 130 ISSN 0264-8172

DOI: 10.1016/j.marpetgeo.2021.105141

The final published version is available online at:

<https://dx.doi.org/10.1016/j.marpetgeo.2021.105141>

Terms of use:

Some rights reserved. The terms and conditions for the reuse of this version of the manuscript are specified in the publishing policy. For all terms of use and more information see the publisher's website.

This item was downloaded from IRIS Università di Bologna (<https://cris.unibo.it/>)

When citing, please refer to the published version.

Validating far-field deformation styles from the Adjara-Trialeti fold-and-thrust belt to the Greater Caucasus (Georgia) through multi-proxy thermal maturity datasets

Sveva Corrado¹, Thomas Gusmeo^{2*}, Andrea Schito^{1,3}, Victor Alania⁴, Onise Enukidze⁴, Enrico Conventi⁵, and William Cavazza²

¹ Dept. of Sciences, Geological Sciences Section, Roma Tre University, Rome, Italy

² Dept. of Biological, Geological and Environmental Sciences, University of Bologna, Bologna, Italy

³ Dept. of Geology and Petroleum Geology, School of Geosciences, University of Aberdeen, Aberdeen AB24 3UE, UK

⁴ Institute of Geophysics, I. Javakhishvili State University, Tbilisi, Georgia

⁵ Geolog Technologies S.r.l. (GEOTech Research and Laboratory) – Viale Ortles 22/4, 20139, Milan, Italy

*corresponding author (e-mail: thomas.gusmeo2@unibo.it; Piazza di Porta San Donato 1, 40126 Bologna, Italy; Tel. +39 0512094545)

Abstract

Thermal history reconstructions can help to better characterise the geological history of areas that experienced a polyphase tectonic evolution. The integration of published stratigraphic/structural data with new and pre-existing data on thermal maturity (clay mineralogy, Raman spectroscopy, vitrinite reflectance, and pyrolysis) of both surface and subsurface sedimentary successions of a wide region of Georgia including -north to south- the southern Greater

Caucasus, the western Kura Basin, and the Adjara-Trialeti fold-and-thrust belt (FTB) provides cogent constraints on its late Mesozoic-Cenozoic tectono-sedimentary evolution.

Overall, thermal maturity spans from the low diagenesis (60-80°C) in the Upper Miocene section of the Kura Basin to anchizone-epizone (about 400°C) in the central Greater Caucasus axial zone. In more detail, different maturity trends and thermal histories point to the existence of two domains formed by positive tectonic inversion: (i) the Adjara-Trialeti FTB from an Eocene rift basin and (ii) the Greater Caucasus from a Mesozoic rift basin. Multiple thermal indicators, along with stratigraphic/structural evidence, show that the Paleocene section of the Adjara-Trialeti basin fill reached the upper oil window (ca. 115°C) during maximum sedimentary burial and that the whole basin was then exhumed starting from the late Middle Miocene. A positive correlation between thermal maturity and stratigraphic age points to a limited thermal effect of tectonic loading. In the southern Greater Caucasus, thermal maturity increases progressively with stratigraphic age, from ca. 100°C (Upper Eocene) to 400°C (Lower Jurassic), in broad agreement with the reconstructed thickness of the basin-fill succession, thus indicating that most of the thermal maturity was again induced by sedimentary burial.

As to the flexural western Kura Basin, its Maikopian (Oligocene-Early Miocene) section reached the oil window (up to ca. 110°C) whereas the Middle-Late Miocene one is immature. The Kakhети ridge -a highly tectonised portion of the Kura Basin- reached immature to early mature conditions.

Keywords

Intra-continental deformation, Alpine orogeny, Maikop, thermal indicators, Caucasus, Kura Basin

1. Introduction

50 The use of indicators of maximum paleo-temperatures and thermal maturity from sedimentary
 51 successions in orogenic zones is traditionally used for hydrocarbon (HC) exploration (e.g. Aldega et
 52 al., 2014; Allen and Allen, 2013; Tozer et al., 2020). Less frequently, it is applied to validate
 53 structural styles in deformed orogenic belts (e.g. Aldega et al., 2018; Atouabat et al., 2020; Balestra
 54 et al., 2019; Caricchi et al., 2015; Di Paolo et al., 2014; Muirhead et al., 2020; Tozer et al., 2020),
 55 either because of lack of constraints on timing of exhumation that can bias thermal modelling, or
 56 because such indicators mostly derive from surface outcrops and can allow modelling only of
 57 pseudo-well sections, rather than present-day boreholes, introducing an extra degree of uncertainty.

58 In recent years the frequent integration of classical and cutting-edge indicators of thermal
 59 maturity due to burial (either sedimentary or tectonic) allowed the assessment of maximum paleo-
 60 temperatures in sedimentary basins with reduced error bars (Corrado et al., 2005, 2020; Goodhue
 61 and Clayton, 2010; Labeur et al., 2021; Liu et al., 2019; Mangenot et al., 2017, 2019; Qiu et al.,
 62 2020; Spina et al., 2018). For example, pyrolysis parameters (HI, PI, Tmax) (Behar et al., 2001;
 63 Tissot et al., 1987), clay-derived geothermometers (such as illite percentage in illite-smectite mixed
 64 layers and illite crystallinity index, KI; Aldega et al., 2007a, 2007b; Schito et al., 2016), vitrinite
 65 reflectance (Balestra et al., 2019; Burnham and Sweeney, 1989; Corrado et al., 2009; Dow, 1977) in
 66 the diagenetic realm and Raman spectroscopy parameters in both the metamorphic and diagenetic
 67 realms on organic matter (Beyssac et al., 2002; Lahfid et al., 2010; Lünsdorf and Lünsdorf, 2016;
 68 Schito et al., 2017) can lead to significant reduction of admissible paleotemperature ranges in the
 69 evolution of compressional areas, especially when they are combined with maximum
 70 paleotemperatures derived from low-T thermochronological modelling [fission-track and (U-
 71 Th)/He dating on apatite crystals] (Aldega et al., 2011; Corrado et al., 2020; Schito et al., 2018).

72 Georgia, located in the deformed hinterland of the Arabia-Eurasia collision occurring along the
 73 Bitlis-Zagros suture zone, represents a privileged and fascinating natural laboratory to validate
 74 structural styles that developed during Arabia-Eurasia convergence using thermal maturity datasets.
 75 Here, different orogenic chains crop out with opposite vergences, variable structural styles and

shortening degrees, accommodating far-field regional convergence (e.g. Adamia et al., 2010, 2011b; Alania et al., 2017; Nemčok et al., 2013). In the present study we consider three tectonic domains: from south to north they are (i) the Adjara-Trialeti FTB, (ii) the Kura Basin (comprising its northern highly deformed portion, the Kakheti ridge) and (iii) the Georgian Greater Caucasus (Fig. 1). Brittle structures and basin sedimentary fills, due to stretching developed either in Mesozoic or early Cenozoic times, influence the geometry and distribution of the late Cenozoic compressive deformation that brought to minor (Kura Basin and Kakheti ridge), moderate (Adjara-Trialeti FTB) or intense exhumation (Georgian Greater Caucasus), with a peak in Miocene times (Alania et al., 2017; Gusmeo et al., 2021; Vincent et al., 2020).

In this region, geometric and genetic relationships between areas affected by positive inversion and moderate to high exhumation, and areas where thin-skinned thrust tectonics develops with higher shortening and less exhumation, are not consistently described (Adamia et al., 2010; Alania et al., 2017, 2018, 2020; Mosar et al., 2010; Nemčok et al., 2013). Different seismic interpretations and scarcity of detailed structural surveys have led to contrasting structural interpretations (Adamia et al., 2010, 2011b; Alania et al., 2020; Banks et al., 1997; Forte et al., 2010, 2013, 2014; Mosar et al., 2010; Nemčok et al., 2013; Tibaldi et al., 2017, 2018). There is also uncertainty regarding the eastward continuation of the Adjara-Trialeti FTB in easternmost Georgia and Azerbaijan, and its link with the unconstrained retrowedge of the Lesser Caucasus (Alania et al., 2017; Nemčok et al., 2013; Sosson et al., 2010, 2016). Moreover, the geometry of the main structural features within the Greater Caucasus, at least in Georgia, is only shown at a crustal scale (e.g. Mosar et al., 2010; Nemčok et al., 2013; Saintot et al., 2006; Sosson et al., 2016). General agreement exists on the nature of a thin-skinned south-verging thrust system in the western portion of the Kura Basin to the south of the eastern Greater Caucasus, where HC exploration and production are ongoing (Alania et al., 2017, 2018; Pace et al., 2019; Pupp et al., 2018).

The purpose of this paper is to give new constraints on the structural style in the three domains of continental deformation in Georgia, to the north of the Bitlis-Zagros suture zone, by presenting and integrating two thermal maturity datasets:

- Surface data, derived from clay mineralogy and Raman spectroscopy, petrography and pyrolysis on organic matter, from Jurassic to Upper Miocene lithostratigraphic units. Original data generated during this study have been integrated by published data from the Kura Basin and the Greater Caucasus.

- Subsurface data, including both published and unpublished results from deep wells exploring the Oligocene-Lower Miocene Maikop series, in the western portion of the Kura Basin and in the easternmost Adjara-Trialeti FTB. These data result from the prolonged attention devoted to the Maikop series, recognised as the main source rock in the Kura Basin (Boote et al., 2018; Pupp et al., 2018). Its oil potential is quite low because of low TOC values and prevalence of type III kerogen (rich in terrestrial input) dispersed in sedimentary rocks. These features extend also to the east moving towards the Caspian Sea (Washburn et al., 2019). Nevertheless, the significant burial depth within the Kura Basin allowed source intervals to enter the oil window in the surroundings of Tbilisi (Pupp et al., 2018; Sachsenhofer et al., 2018).

The integration of the two datasets with the tectono-stratigraphic setting of the three main structural domains, derived from original field surveys and pre-existing literature, allowed (i) to constrain the level of thermal maturity acquired through time in the extensional and flexural basins considered, and (ii) to evaluate the relative contribution of sedimentary/tectonic burial to the thermal maturation during extensional phases and intraplate shortening, a few hundred kilometres to the north of the Bitlis-Zagros suture zone of the Arabia-Eurasia collision (Cavazza et al., 2018, 2019).

2. Geological Setting

125

126 The study area is located in eastern Georgia and covers (i) the easternmost Adjara-Trialeti fold-
 127 and-thrust belt, (ii) the southern (Georgian) side of the central Greater Caucasus orogen (GC), (iii)
 128 the westernmost Kura Basin (including the Kakheti ridge, a structural culmination developed in its
 129 northern sector) (Fig. 1).

130 The Adjara-Trialeti FTB is an orogen bordered mainly by north-vergent frontal reverse faults
 131 (Alania et al., 2018; Banks et al., 1997; Gusmeo et al., 2021; Nemčok et al., 2013) and resulting
 132 from the structural inversion of a former back-arc rift basin developed on the upper (Eurasian) plate
 133 of the northern Neotethys subduction zone (Adamia et al., 1981, 2011b; Banks et al., 1997; Barrier
 134 et al., 2018; Lordkipanidze et al., 1989). The main phase of rifting occurred in the Middle Eocene,
 135 characterized by the deposition of a thick volcanic and volcanoclastic succession, accompanied by
 136 shallow mafic-to-intermediate intrusions (Adamia et al., 2011b; Banks et al., 1997; Okrostsvadze
 137 et al., 2018; Yilmaz et al., 2000, 2014). The post-rift phase lasted from the Late Eocene/Oligocene
 138 to the Early Miocene and was followed by structural inversion since late Middle Miocene times
 139 (Gusmeo et al., 2021). The Adjara-Trialeti FTB is often considered as part of the retro-wedge of the
 140 Lesser Caucasus orogen *s.l.*, despite having an independent origin (Alania et al., 2017; Mosar et al.,
 141 2010; Nemčok et al., 2013; Yilmaz et al., 2014).

142 The Greater Caucasus orogen is a fold-and-thrust belt resulting from the inversion of a back-arc
 143 rift basin (Greater Caucasus Basin) which opened in the Early Jurassic (Adamia et al., 1981, 2011a,
 144 2011b; Dercourt et al., 1986; Mosar et al., 2010; Nikishin et al., 2001; Saintot et al., 2006;
 145 Sobornov, 1996; Zonenshain et al., 1990). Rifting is marked by Hettangian-Sinemurian black shales
 146 nonconformably overlying the crystalline basement, followed by siliciclastic turbidites, lavas and
 147 volcanoclastics deposited until the late Middle Jurassic; volcanic products were mostly deposited
 148 from Aalenian to Bajocian times (Adamia et al., 2011a, 2011b; Lordkipanidze et al., 1989; Nikishin
 149 et al., 2001; Saintot et al., 2006). From the latest Middle Jurassic until the Late Eocene the basin
 150 experienced post-rift thermal subsidence, characterized by the deposition of calcareous and

151 siliciclastic turbidites (Adamia et al., 2011a, 2011b; Saintot et al., 2006; Zonenshain et al., 1990).
 152 The Greater Caucasus Basin was probably underlain by thinned continental crust rather than
 153 oceanic crust (Ershov et al., 2003).

154 There is an ongoing debate regarding the timing of structural inversion of the Greater Caucasus
 155 Basin and subsequent development of the Greater Caucasus orogen, with hypotheses ranging from
 156 the earliest Oligocene (Lozar and Polino, 1997; Nikishin et al., 2017; Vincent et al., 2007, 2013a,
 157 2013b, 2016) to the Middle Miocene (Rolland, 2017) to the Pliocene (Avdeev and Niemi, 2011;
 158 Cowgill et al., 2016; Forte et al., 2014; Philip et al., 1989). Low-temperature thermochronology
 159 data seem to suggest an earlier growth of the western Greater Caucasus (e.g. Vincent et al., 2011)
 160 with respect to the eastern and central parts of the orogen (e.g. Avdeev and Niemi, 2011; Vasey et
 161 al., 2020; Vincent et al., 2020). The central and eastern portions of the Greater Caucasus certainly
 162 underwent rapid Pliocene to recent uplift. There is no consensus on the causes of such a fast
 163 exhumation (see for example the discussion in Vincent et al., 2020). Anyway, most authors agree
 164 that at least about 5-8 km of Cenozoic uplift occurred in the Greater Caucasus.

165 Convergence between the Greater Caucasus and the Lesser Caucasus, namely the Adjara-Trialeti
 166 FTB in the study area, caused the development of the so-called Transcaucasian intermontane
 167 depression, constituted by the Kura and Rioni flexural foreland basins, plunging to the east and
 168 west, respectively, and separated by the Dzirula Massif (Adamia et al., 2010, 2011b; Alania et al.,
 169 2017; Banks et al., 1997; Nemčok et al., 2013; Rolland et al., 2011). The two basins developed as a
 170 flexural response to both the Greater Caucasus to the north and the Lesser Caucasus *s.l.* to the
 171 south, and are filled by Oligocene-to-recent sediments (Fig.2) (Adamia et al., 2010; Banks et al.,
 172 1997; Nemčok et al., 2013). The Kartli Basin (Figs. 1 and 2) is considered as a sub-basin of the
 173 Kura foreland basin bordered by the Adjara-Trialeti FTB to the south and the Greater Caucasus to
 174 the north. In the Kura Basin, the Maikop series is composed of Oligocene-Lower Miocene clastic
 175 (shales, siltstones and fine-grained sandstones) and evaporitic rocks deposited in the anoxic-dysoxic
 176 environment of the Paratethys (Pupp et al., 2018; Sachsenhofer et al., 2018). The thickness of the

177 Maikop series can reach 2.5-3.5 km in some parts of the Kura Basin (Adamia et al., 2010). During
 178 Middle to early Late Miocene times further 1.5-2.2 km of shales and fine-grained siliciclastics
 179 (sandstones), intercalated in the uppermost sections with mainly calcareous units (mudstones, marls
 180 and oolitic limestones and locally with coarse-grained rocks), were deposited within the Kura Basin
 181 (Adamia et al., 2010; Alania et al., 2017). Since the Tortonian, the western part of the basin has
 182 been under subaerial conditions and marine conditions persisted only in some localities and in the
 183 easternmost portion of the basin (Adamia et al., 2010; Barrier et al., 2018). At the same time the
 184 widespread deposition of coarse-grained clastic deposits, eroded from the adjacent orogenic belts,
 185 started. Continental conditions prevailed from the Late Sarmatian (i.e. Tortonian, Fig. 2; see
 186 Adamia et al., 2010; Lazarev et al., 2019; Neubauer et al., 2015 for a review) to the present,
 187 interrupted only in the late Pliocene by a short-lived shallow marine environment, probably in
 188 response to the rapid growth and advancement of the Greater Caucasus and the ensuing subsidence
 189 in the foreland area (Adamia et al., 2010; Avdeev and Niemi, 2011; Nemčok et al., 2013;
 190 Sukhishvili et al., 2020).

191 Nemčok et al. (2013), based on the geometry of the sedimentary wedges, recognized a multi-
 192 stage development of the Kura foreland basin. In Oligocene times the depocenter was located along
 193 the SW border with the sedimentary fill thinning progressively towards the NE. In Early-Middle
 194 Miocene times maximum subsidence switched to the NE, with a clastic wedge progressively thinner
 195 and finer grained from NE to SW, indicating that the basin was being flexed in response to the
 196 southward advance of the Greater Caucasus. Since the Late Sarmatian (Tortonian) ongoing
 197 convergence between the Greater and Lesser Caucasus forced the final uplift of the Dzirula Massif
 198 and the Kura Basin started plunging towards the Caspian Sea, as demonstrated by the progressive
 199 emergence of the basin from west to east (Adamia et al., 2010; Alania et al., 2017; Nemčok et al.,
 200 2013). Symmetrically, the Rioni Basin plunged towards the Black Sea, on the western side of the
 201 Dzirula Massif. Thus, the Dzirula Massif basement high separated definitely the Rioni Basin from
 202 the Kura Basin (Banks et al., 1997; Barrier et al., 2018; Shatilova et al., 2020).

Continued convergence between the Greater and Lesser Caucasus caused incremental deformation of the Kura foreland basin. Thick-skinned deformation occurred in the Early-Middle Sarmatian (late Serravallian-early Tortonian) followed by thin-skinned deformation from the Late Sarmatian-Meotian (Tortonian) onward (Nemčok et al., 2013). During convergence, the Greater Caucasus deformation propagated into the northern Kura Basin forming the Kura south-vergent thin-skinned foreland FTB (Kakheti ridge), starting from the Middle Miocene, with peak deformation in the Late Miocene-Pliocene (Alania et al., 2017). A Late Pliocene-Pleistocene acceleration of uplift occurred also in this belt (Sukhishvili et al., 2020), probably linked with coeval enhanced uplift in the Greater Caucasus and subsequent propagation of deformation. The south-verging structures due to the southward growth of the frontal Greater Caucasus and the north-verging Adjara-Trialeti FTB structures interfere in the Tbilisi area, creating an outstanding example of incipient collision between two oppositely verging orogenic belts (Alania et al. 2021; Fig. 1).

3. Materials and Methods

3.1 Materials

Both outcrop samples and cuttings from wells were analysed to assess thermal maturity and TOC content, when available, in the study area (Tables 1 and 2). Samples were analysed using several techniques and results were integrated with published data available for the study area for the first time in this paper (Figs. 1 and 3). Data from Bujakaite et al. (2003), Pupp et al. (2018) and Samsu (2014) are presented in the Results section (Tables 1 and 2), whereas other published data are integrated in the Discussion section.

More than two hundred subsurface TOC and Tmax data were derived from seven wells drilled in the eastern Adjara-Trialeti FTB and in the western Kura Basin (where HC exploration is

concentrated), from which we extrapolated the Oligocene-Early Miocene interval (Maikop series) in order to have a reference section for interpretation. Pyrolysis results and TOC content estimates were made using Rock-Eval technology and ELTRA Elementar Analyser, respectively. Details on the methods are provided in Pupp et al. (2018) and Samsu (2014). From south to north the wells are (Fig.1):

- I. Kumisi 2
- II. Patardzeuli (SLB)
- III. Satskhenisi 102
- IV. Norio 200
- V. Norio 72
- VI. Ninotsminda 97
- VII. Manavi 12

About forty surface samples (Table 1) were analysed or revised in the three geological domains from various stratigraphic intervals: Jurassic (original data and after Bujakaite et al., 2003); Cretaceous (original data); Late Paleocene-Eocene (original data and after Pupp et al., 2018); Oligocene-Early Miocene (original data and after Pupp et al., 2018); Middle-Late Miocene (original data). They were characterised using organic petrography, pyrolysis and micro-Raman analyses on dispersed organic matter, and XRD diffraction on the <2 µm fraction of clay minerals.

3.2 *Methods*

3.2.1 *Organic petrography*

Vitrinite reflectance (VRo%) is generally the best thermal indicator in sedimentary sequences rich in organic matter, and can be correlated with detailed stages of HC generation (Bertrand et al., 2010; Borrego and Cook, 2017; Dow, 1977).

Preparation of the samples for optical microscope analysis of dispersed organic matter and vitrinite reflectance required picking of the visible organic matter particles, that can be easily found in the silty and arenaceous fractions, often as vegetable whips (Barnes et al., 1990; Taylor et al., 1998). Once a few grams of rock containing organic matter were selected, they were smoothly crushed in an agate mortar to a medium sand grain size. Obtained powder was placed on a sample holder and incorporated in a two-component epoxy resin. Then specimens were sanded using a Struers LaboPol 5 automatic sanding/polishing machine, with 320, 500 and 1000 grit carborundum sandpaper, and isopropanol lubricant and water as coolers. Then specimens were finally polished with alumina suspensions, with decreasing grain size (1 to 0.3 μm) and microfibre cloths. The routine was completed by polishing with 0.12 μm fumed silica suspension.

Vitrinite reflectance analysis was performed at the ALBA (Academic Laboratory of Basin Analysis) of Roma Tre University using a Zeiss Axioskop 40 A microscope equipped with a tungsten halogen lamp (12V, 100W) that produces non-polarized light ($\lambda = 546 \text{ nm}$), Epiplan-Neofluar 50x/1 objective immersed in oil ($n = 1.518$) at a temperature of 23°C, photomultiplier MPS 200 (from J & M Analytik AG), short- and long-wave ultraviolet lamps, coupled with a Canon Power Shot G6 digital camera and a dedicated software for reflectance data acquisition.

Before starting measurements, instrument calibration was performed with three reflectance standards. In addition, parasitic light intensity (which varies depending on the intensity of sunlight throughout the day) was measured to allow the software to filter it.

The average vitrinite reflectance (VRo%) values were calculated as the arithmetic mean over a minimum of 20 measurements per sample and considered acceptable with a maximum standard deviation of ± 0.06 on the indigenous fragments (Borrego et al., 2006). Each measurement was

made on well preserved non-oxidised fragments $>5\ \mu\text{m}$ and as far as possible from fractures and pyrite crystals that could decrease or increase true reflectance values, respectively.

3.2.2 *Micro-Raman spectroscopy on dispersed organic matter*

Raman spectroscopy is a non-destructive tool to quantitatively evaluate thermal maturity of organic matter from diagenesis to metamorphism (Beyssac et al., 2002; Ferralis et al., 2016; Guedes et al., 2010, 2012; Henry et al., 2019; Hinrichs et al., 2014; Lahfid et al., 2010; Liu et al., 2013; Lünsdorf and Lünsdorf, 2016; Mumm and Inan, 2016; Quirico et al., 2005; Schito et al., 2017, 2019; Schito and Corrado, 2018; Wilkins et al., 2014; Zhou et al., 2014). Advances in instrumentation and data processing have spurred increased applications, and the technique is now simple, fast and can be performed directly on standard petrographic thin sections or on bulk kerogen.

Raman spectra were acquired at the laboratory of experimental volcanology and petrology (EVPLab) of Roma Tre University on standard petrographic thin sections following the procedure described by Beyssac et al. (2002) and Lünsdorf et al. (2017). The spectrometer used is a Jobin Yvon micro-Raman LabRam with a backscattered geometry in the range of $700\text{--}2200\ \text{cm}^{-1}$ (1st order Raman spectrum), which uses a grid of 600 meshes per mm and a CCD detector with a maximum magnification of 50x. A Nd-YAG laser with a wavelength of 532 nm (green laser) with a power $< 0.4\ \text{mW}$ was used as energy source. Raman back scattering was then recorded in six repetitions with 20-second steps for each measurement which, together with the use of green lasers and optical filters, helped to reduce the background noise given by the fluorescence of organic matter within acceptable values (Schito et al., 2017). A total of twenty measurements were made for each sample to ensure reproducibility using a $2\ \mu\text{m}$ diameter spot at 50x magnification.

An automatic approach (Ifors software) was followed for the identification of the number of bands of the Raman spectrum, as illustrated by Lünsdorf et al. (2017) and Lünsdorf and Lünsdorf

(2016). The method is based on the STA (Scaled Total Area) parameter, which is a function of the area and maximum intensity of the D and G peaks (Fig. 4). Once this parameter is calculated, using a 532 nm green laser source, it is possible to obtain the maximum burial temperatures by solving the following equation:

$$T_{532 \text{ nm}} [^{\circ}\text{C}] = -8,259 \cdot 10^{-5} \cdot \text{STA}^3 + 3,733 \cdot 10^{-2} \cdot \text{STA}^2 - 6,445 \cdot \text{STA} + 6,946 \cdot 10^2.$$

3.2.3 XR diffraction on <2 μm grain-size fraction

Clay minerals in shales and sandstones undergo diagenetic and very low-grade metamorphic reactions in response to sedimentary and/or tectonic burial. In particular, mixed layers illite-smectite (I-S) and the transformation sequence smectite-randomly ordered mixed layers (R0)-ordered mixed layers (R1 and R3)-illite-muscovite (di-octahedral K-mica) can be used as indicators of the thermal evolution of sedimentary successions (Aldega et al., 2007a, 2007b, 2014; Pollastro, 1990).

Illite crystallinity (IC) is the measure of the full width at half maximum (FWHM) of the first illite diffraction peak ($1 \text{ nm} = 10 \text{ \AA}$) and is a method suitable to detect the anchizonal and its immediate limits, for which it is most accurate (Kübler and Jaboyedoff, 2000).

Samples were analysed for qualitative and semi-quantitative analyses of the <2 μm grain size fraction at Roma Tre XRD Laboratory. X-Ray diffraction (XRD) analyses were carried out with a Scintag X1 X-ray system ($\text{CuK}\alpha$ radiation) at 40 kV and 45 mA. Randomly oriented whole-rock powders were run in the $2\text{--}70^{\circ} 2\theta$ interval with a step size of $0.05^{\circ} 2\theta$ and a counting time of 3s per step. Oriented air-dried and ethylene-glycol solvated samples of the <2 μm (equivalent spherical diameter) grain-size fraction were scanned from 1 to $48^{\circ} 2\theta$ and from 1 to $30^{\circ} 2\theta$, respectively, with a step size of $0.05^{\circ} 2\theta$ and a count time of 4s per step.

The illite content in mixed-layers I-S is determined by the delta two-theta method after decomposing the composite peaks between $9\text{--}10^{\circ} 2\theta$ and $16\text{--}17^{\circ} 2\theta$ (Moore and Reynolds, 1997)

and by modelling XRD patterns using Pearson VII functions. The R ordering of I-S (Reichweite parameter, R; Jagodzinski, 1949) is determined by the position of the I 001-S 001 reflection between 5 and 8.5° 2 θ .

‘Illite crystallinity’ (IC, also called Kübler Index, KI) measurements are made by first subtracting the background from the raw data, and then applying a profile-fitting method (Lanson, 1997). The 10 Å asymmetric illitic multiphase peak was fitted using the Scintag X1 software. Peak shape decomposition was performed on ethylene-glycol preparations using split Pearson VII functions. The peaks identified were rationalized in terms of specific discrete or mixed-layers I-S and/or C-S phases (Lanson, 1997). From fitted data, the crystallinity was determined after calibrating the full width at maximum height (FWHM) of the illite band using Warr and Rice (1994) standards. According to the classification of Kübler (1964), KI values between 0.42 and 0.25 correspond to the anchizone (200-300°C) while values lower than 0.25 reflect the onset of epizone at temperatures higher than 300°C.

3.2.4 Correlation among different indicators of maximum temperature exposure

Correlation among different thermal indicators and conversion into temperatures are not straightforward since the different factors that drive maturation in sedimentary basins such as thermal regime, sedimentation rate, tectonic subsidence, mineral availability and fluid circulation dissimilarly affect each analytical parameter. Nevertheless, to provide a broad view of the temperature variation among and within the different basins (Fig. 5), we attempted a conversion of organic indicators using the most accepted equations or correlations, i.e. Barker and Pawlewicz (1986) for vitrinite reflectance and vitrinite reflectance equivalent from T_{max} values, and Lünsdorf et al. (2017) for Raman parameters. T_{max} values were preliminary converted into vitrinite reflectance equivalent using Barnard et al. (1981). I% in I-S were converted according to Aldega et

al. (2007b) and Merryman and Frey (1999). Throughout the paper, we consider the classical temperature range established for the oil window (ca. 90-120°C, see Hartkopf-Fröder et al. (2015) and references therein). VRo% and I% in I-S were plotted on Hillier et al.'s diagram (1995), where each couple of data can be attributed to different heating rates, that in turn can be ascribed to different geodynamic settings characterised by low (e.g. cratons or foreland basins) to very high (e.g. rift basins) thermal regimes.

4. Results

Results are analytically provided in Tables 1 and 2 and synthesized in Figs. 3 and 5.

4.1 Organic petrography

Vitrinite reflectance and main petrographic observations of new surface samples from the Adjara-Trialeti FTB, the Kura Basin and the Kakheti ridge (Table 1) are described below; no data are provided for the Greater Caucasus because the high maturity levels in this domain prevented accurate VRo% determination.

The Maastrichtian-Danian to Oligocene-Lower Miocene samples collected in the Kakheti ridge show a decrease in thermal maturity from the oil window (VRo about 0.65%) to the immature stage of hydrocarbon generation (VRo 0.48%). Only three out of five samples provided reliable reflectance values, given the scarcity of OM and the diffuse presence of macerals belonging to the inertinite group, useless for maturity studies. Samples CA20 and CA28 show the most reliable results given the high content of in-situ vitrinite (more than 40 fragments) and the low standard deviation. The presence of yellow and UV-fluorescent sporinites confirms the low maturity level.

Three Oligocene-Miocene samples (CA15, CA16 and CA17) from the Kura Basin are characterised by a high content in terrestrial debris with minor amount of inertinite and semifusinite fragments. Vitrinite reflectance measurements indicate as a whole the immature stage of hydrocarbon generation, with VRo values ranging from 0.40 to 0.49% and very low standard deviation values.

Finally, seven Paleogene samples from the Adjara-Trialeti FTB were analysed. Organic facies are mainly composed by huminite-vitrinite group fragments with minor amount of inertinite fragments and some sporinites. Pyrite is frequent in globular aggregates of variable sizes. Measured vitrinite reflectance ranges between 0.50 and 0.77% indicating the early and middle oil window stage.

4.2 New and revised Tmax and TOC data from pyrolysis

Presented Tmax and TOC data generally derive from the Oligocene-Lower Miocene Maikop interval, drilled in seven wells located in the eastern surroundings of Tbilisi (Figs. 1 and 3). They are from unpublished reports produced for the Georgia Oil & Gas Company and from Samsu (2014).

Further surface data derive from new sampling along the Kakheta ridge, the Dzirula Massif and the more external units of the Greater Caucasus, whereas data from Pupp et al. (2018) come from the easternmost Adjara-Trialeti FTB and the Kura Basin. They have been selected in order to integrate our new original maturity and obtain the maturity distribution shown in the map of Fig. 3.

Tmax values of samples with less than 0.5% TOC were disregarded. Kerogen is mostly type III to type II-III (Fig. 6), with substantial input of terrestrial organic debris. Maturity falls in the diagenetic realm ranging from the immature (<0.5% VRo) to the mid-mature and, rarely, late mature stages of HC generation. Thermal maturity is generally lower in younger (Maikop) with

respect to older (Upper Eocene and Cretaceous) stratigraphic intervals (Fig. 6). Analytical data are presented in Tables 1 and 2 and in Figure 7.

In detail, the sampled Maikop section in the Kumisi 2 well ranges between 1340 and 1535m depth with a Tmax between 434 and 441°C and a mean value of 439°C, and with TOC ranging between 1.05 and 1.95% with a mean of 1.44% (Fig. 7).

In the Patarzeuli (SLB) well, sampled between 360 and 1350m depth, Maikop Tmax ranges between 422 and 440°C with a mean of 431°C, whereas mean TOC is around 1% with minimum and maximum values of 0.64 and 1.25%, respectively (Fig. 7).

In the Satskhenisi 102 well, sampled between 200 and 1200m depth, over 80% of the Maikop samples have TOC values higher than 1%, with a minimum value of 0.50% and a maximum one of 2.40%. There is no clear TOC trend with depth. Nevertheless, the highest TOC values (>2%) are concentrated towards the bottom half of the section (below 700m of depth) (Fig. 7).

The Oligocene interval in the Norio200 well, between 665 and 1233m depth, shows a Tmax between 423 and 429°C with a mean of 427°C, and TOC ranging between 1.75 and 2.19% with a mean of 1.93% (Fig. 7).

In the Norio72 well, the Maikop (3625-4510m) yielded Tmax comprised between 418 and 435°C with a mean value of 427°C, and TOC ranging between 0.30 and 1.60% with a mean of 0.80% (Fig. 7).

In the Ninotsminda 97 well the Lower Oligocene interval of the Maikop (2330-2360m) yielded Tmax values between 421 and 424°C with a mean of 422°C. TOC ranges between 0.63 and 0.82%, with a mean of 0.76%.

The Manavi 12 well crosses the Maikop between 3800 and 3920m depth with Tmax indicating the immature stage of HC generation (between 407 and 431°C with a mean of 424°C), and TOC between 3.30 and 5.40% with a mean of 4.20%.

New surface samples collected along the Kakheta ridge and the frontal tectonic units of the Greater Caucasus show higher Tmax values in the latter ones (mainly >450°C in Upper Eocene

rocks and 445°C in the Cenomanian sample CA35). In the Kakheti ridge Late Eocene Tmax ranges between 434 and 442°C and Oligocene-Miocene Tmax ranges between 421 and 427°C, suggesting a lateral trend of decreasing maturity moving from the WNW to ESE and an increase of maturity from younger to older strata.

Original surface data from the Cretaceous unconformably lying on top of the Dzirula massif indicate a Tmax lower than 437°C.

Surface sections studied by Pupp et al. (2018) between the Adjara-Trialeti FTB and the Kura Basin provide reliable Tmax data for the Late Eocene-Oligocene (446-448°C), Late Oligocene-Miocene (429-435°C) and Miocene (<437°C) intervals, showing an overall maturity decrease from older to younger units. Oligocene sample CA4, collected in the Akhaltsikhe depression, yielded a Tmax value of 430°C.

4.3 Raman spectroscopy on dispersed organic matter

Measurements of Raman spectra on dispersed organic matter were focused on samples from the Greater Caucasus, where metamorphic temperatures make vitrinite reflectance data less reliable for thermal maturity assessments. Here, Raman spectra show a clear-cut temperature increase going from the younger to the older chronostratigraphic units as well as toward the axis of the orogen (Table 1). This trend is illustrated in Fig. 4, where spectra from Lower Jurassic to Middle Cretaceous samples collected along a N-S transect running parallel to the Georgian Military Road are shown. Upper Jurassic sample CA39 crops out a few tens of km to the ESE of it and thus its thermal evolution should be considered separately from the other samples; for this reason, the Raman spectrum of this sample is not included in Fig. 4.

Spectra from Aptian to Cenomanian successions (samples CA36 and CA37), as well as in Upper Jurassic sample CA39, are characterised by a broad asymmetric D band at 1350cm⁻¹ with lower

intensities with respect to the G band at 1600cm^{-1} . Such spectra are typical of very low metamorphic conditions, as outlined by the temperature range from the Ifors software ($219\text{-}235^\circ\text{C}$). Moving toward the Berriasian-Hauterivian sample (CA38) the D band shows relatively higher intensities and the bands that underlines the “saddle” between the D and G bands tend to disappear. These changes reflect a temperature increase up to $292 \pm 7^\circ\text{C}$, near the boundary between anchizone and epizone ($\sim 300^\circ\text{C}$ according to Kübler, 1964). Finally, in the Jurassic sample (Toarcian-Aalenian, CA40) the intensity of the D band is higher than that of the G band, which shows a marked asymmetry at 1620cm^{-1} due the presence of the D2 band. All these features correspond to an average temperature of $379 \pm 9^\circ\text{C}$.

4.4 XRD on $<2\ \mu\text{m}$ grain-size fraction

Data obtained from clay mineralogy analyses are shown in Table 1. The interpretation of diffractograms on air-dried and glycolated samples are expressed as abundance in percentage to provide the composition of the $<2\ \mu\text{m}$ fraction. Moreover, where illite-smectite (I-S) mixed layers are present, the percentage of illite in mixed layers (I% in I-S), which can be interpreted in terms of maximum temperature, and the parameter R (Reichweite index) are provided. IC (illite crystallinity) is provided for samples where only illite (without I-S mixed layers) is present.

In the Greater Caucasus, three samples (CA36, CA37 and CA38) contain 8 to 28% of I-S mixed layers, together with illite (1-88%) and chlorite (6-71%). These samples have a R3 stacking order of illite-smectite mixed layers and I% in I-S ranging from 80% (Cenomanian, CA36) to 88% (Aptian-Albian, CA37), indicating the late diagenetic realm. The remaining two samples from the Greater Caucasus, CA40 (Toarcian-Aalenian) and CA39 (Oxfordian-Tithonian), contain illite, chlorite and chlorite-smectite mixed layers. According to Kübler's (1964) classification, IC values of the Lower Cretaceous (CA38) and the Lower-Middle Jurassic (CA40) samples indicate respectively anchizone

and epizone conditions whereas the Upper Jurassic sample (CA39), located >70 km to the ESE, reached only late diagenetic conditions.

The six samples from the Kakheti ridge of the Kura Basin contain I-S mixed layers (generally >20%), illite (30-65%), chlorite (2-30%) and kaolinite (10-30%), with the exception of the Maastrichtian sample where these last two phases are absent. Kaolinite -indicative of intense weathering- is virtually absent in samples from other domains. I% in I-S mixed layers ranges mainly between 70 and 75%, with R1 stacking order. Two samples (CA28, Maastrichtian, and CA19, Oligocene-Early Miocene), collected near two fault zones, show much lower I% in I-S mixed layers (18 and 15%, respectively) probably due to alteration that could increase the smectite percentage.

Two Miocene samples from other areas of the Kura Basin provided reliable XRD results, indicating low diagenetic conditions. CA14 (Late Miocene) contains mainly smectite (85%) and minor amounts of illite and chlorite (10 and 5%, respectively). CA16 (Early Miocene) contains illite, chlorite, illite-smectite mixed layers (<20%) with a percentage of illite in mixed layers of 45% and R0 stacking order. The abundance of kaolinite (>30%) indicates weathering processes.

Almost all of the eight samples from the Paleogene section of the Adjara-Trialeti FTB contain chlorite-smectite mixed layers, nearly absent in the other domains, with percentages ranging from about 20 to 80%. Illite is ubiquitous with highly variable percentages (5-72%), and chlorite is frequently present, with a lower percentage in the Paleocene-Early Eocene sample (CA13, 6%) than in the Eocene section (28-33%). I-S mixed layers are present only in four samples in the Eocene section, with percentages between 24 and 40%. I% in I-S mixed layers is highly variable, with two samples (CA11 and CA7, Early and Late Eocene, respectively) yielding a percentage between 70 and 76% and R1 stacking order, and two samples (CA10 and CA9, Middle and Late Eocene, respectively) with I% between 27 and 32% and R0 stacking order.

4.5 *Extrapolation of paleotemperature ranges and integration with pre-existing datasets*

Organic indicators (VRo% and Tmax from pyrolysis) from virtually all of the Paleocene-Miocene samples of the Adjara Trialeti FTB point consistently to the diagenetic realm (early to mid-mature stages of hydrocarbon generation), thus never exceeding about 115°C. I% in I-S and R ordering show, on the other hand, contrasting values (Table 1). Considering organic results, we suggest that the two samples (CA8 and CA9) with low I% in I-S mixed layers and R0 ordering have probably been affected by alteration processes (hence these two samples were not plotted on Fig. 8). In the Hillier's (1995) diagram (Fig. 8) the correlation between VRo% and I% in I-S for sample CA11 indicates a medium heating rate during back-arc extension in the eastern Adjara-Trialeti basin, before inversion.

The three Oligocene-Miocene samples from the Kura Basin yielded coherent paleotemperatures between 60 and 80°C, based on VRo% and I% and stacking order of I-S mixed layers (Fig. 5). The correlation between VRo% and I% in I-S for sample CA16 indicates a moderate heating rate typical of relatively cold basins (Fig. 8). This is further confirmed by Tmax values from the Oligocene-Early Miocene Maikop unit, or part of it, in the wells near Tbilisi (Figs. 1, 3 and 6, Table 2), indicating that the maturity trend with depth defines cold conditions, and by Pupp et al. (2018) who define a maturity gradient of 0.08%/km (Δ VRo%) in the Maikop series, typical of cold foreland basins. The new pyrolysis results (Tmax, TOC and HI; Tables 1 and 2, Figs. 6 and 7) also show that the organic matter is mainly of type III to type II-III, thus rich in terrestrial input: this evidence and the maturity level reconstructed are in agreement with published results from wells and outcrop samples in the western Kura Basin (Pupp et al., 2018; Samsu, 2014).

The thermal maturity of the Cretaceous sample (CA18) collected at the surface from the unconformable cover of the Dzirula Massif indicates shallow burial.

As for the Kakheti ridge, all reliable data fall in the diagenetic realm showing a general increase of paleotemperatures derived from organic indicators (T_{\max} and $V_{\text{Ro}}\%$) from 40-50°C to about 100°C moving from younger (Oligocene-Lower Miocene) to older (Lower Cretaceous) lithostratigraphic units (Figs. 5 and 6). XRD analysis of the $<2\ \mu\text{m}$ fraction indicates the presence of I-S mixed layers with an illite content of more than 70% and R1 ordering. These results suggest a much higher thermal maturity with respect to $V_{\text{Ro}}\%$ and T_{\max} that can be interpreted as detrital clay contamination. On the other hand, two samples collected close to thrusts show a much lower illite content in mixed layers ($<20\%$) probably due to post-diagenetic smectite enrichment caused by fluid circulation. Hillier's diagram (Fig. 8) indicates a low to moderate heating rate, typical of relatively cold basins (samples CA27-CA20).

In the Greater Caucasus, Raman spectroscopy and XRD (KI and I% in I-S) in the axial part of the belt, and T_{\max} in the southern foothills provided new reliable results (Figs. 5 and 9). In the Lower Jurassic section sampled on the highest thrust sheet of the Greater Caucasus close to the Russia-Georgia border, the maximum paleotemperatures derived from XRD and Raman are comprised between 300 and 400°C, with a more refined range given by Raman spectroscopy (360-400°C, Figs. 4 and 5). Raman results should be privileged as KI-derived paleotemperatures result from a discontinuous correlation scale (Hoffman and Hower, 1979) whereas the equation used to calculate temperatures from Raman parameters (Lünsdorf et al., 2017) provides a more detailed resolution. Additional KI data (Bujakaite et al. (2003) confirm that maximum paleo-temperatures were higher than 300°C. These results are further corroborated by thermochronological results from Vasey et al. (2020), indicating that the basement in the axial zone of the Greater Caucasus near Mt. Kazbek (Fig. 1) underwent very fast cooling since about 10-8 Ma from temperatures higher than ~250°C.

Moving to the footwall of the highest thrust, KI data indicate a decrease in paleotemperatures from more than 300 to about 250°C going upsection from north (Lower Jurassic) to south (Upper Jurassic) (Bujakaite et al., 2003).

New Raman, KI, Tmax and I% in I-S data from the bottom of the Cretaceous succession indicate a well constrained range between 280 and 300°C, that decreases to 180-260°C moving towards the uppermost Lower Cretaceous and Cenomanian units. Here the percentage of illite probably slightly underestimates paleotemperatures for lithological reasons (abundant carbonate cement) whereas R3 stacking order suggests paleotemperatures partially superposing with Raman ones.

In the southern foothills of the Greater Caucasus, an area dominated by thin-skinned thrust sheets, Tmax values suggest a paleotemperature range between 100 and 160°C in the Upper Eocene rocks, corroborated by the Tmax vs HI relationships (Fig. 6) which indicate a late mature to overmature stage of HC generation. These results show that the youngest stratigraphic units in the orogenic belt are characterised by the lowest maturity level.

Overall, the integration of the new data presented here with pre-existing datasets describes a progressive increase of thermal maturity from the southernmost foothills to the highest peaks of Greater Caucasus in Russian territory, i.e. from younger to older strata (Figs. 5 and 9).

5. Discussion

5.2 Thermal histories

The thermal maturity distribution for the three geological domains characterising the study area is represented in Fig. 5 and along the profile in Fig. 9. In the Paleocene-Lower Eocene section of the Adjara-Trialeti FTB, thermal maturity decreases from south (Tetri Tsqaro) to north (Mtskheta), from the peak of the oil window to the early mature zone. The difference in thermal maturity is relatively small but could be explained with the possible effect of tectonic thickening due to the inverted E-W fault running in the area of Amlevi, evolving into a low-angle thrust in its present-day eroded portion (Figs. 1, 3 and 9).

579 The thermal maturity of the Middle-Upper Eocene section does not show significant relevant
580 lateral variations. It ranges from the immature stage of HC generation to the oil window and is
581 slightly lower in comparison with the Paleocene-Eocene section.

582 The thick Oligocene-Lower Miocene (Maikop) section of the Adjara-Trialeti FTB reached the
583 early mature oil window, whereas it is immature in the central portion of the orogen [samples CA1
584 and CA2 (Pupp et al., 2018)]. Further to the north, where the Maikop series is overlain by Middle-
585 Upper Miocene sediments in the frontal synform of the Adjara-Trialeti FTB (Figs. 3 and 9), thermal
586 maturity increases again to the early mature stage. The thermal immaturity of the Maikop section in
587 the Kumisi 2 well could be explained with the closure of the former Adjara-Trialeti back-arc basin
588 towards the SE, hence to the lower amount of experienced burial (Fig. 3).

589 The positive correlation between thermal maturity and stratigraphic age suggests the limited
590 effect of tectonic loading, apart for the southern part of the cross-section in Fig. 9. Maximum
591 temperatures recorded in the Adjara-Trialeti domain are consistent with the thickness of the rift
592 basin fill and hence resulted from sedimentary burial. The thermal maturity trend reconstructed in
593 the Adjara-Trialeti FTB thus provides independent evidence that the dominant deformation style
594 within the orogen is positive inversion of the former extensional faults, as already pointed out in
595 previous works (Alania et al., 2020; Banks et al., 1997; Gusmeo et al., 2021; Sosson et al., 2016),
596 rather than low-angle thrusting, a process which would have resulted in a higher thermal maturity
597 due to tectonic overburden.

598 Based on our results, suggesting maximum paleotemperatures between about 70 and 120°C, and
599 assuming an average geothermal gradient of 25-30°C/km, the total eroded basin fill of the eastern
600 Adjara-Trialeti Basin broadly ranges between 2 and 4.5 km. These rough estimates are in agreement
601 with Pupp et al. (2018), who estimated ~3/3.5 km of eroded Miocene section in the eastern Adjara-
602 Trialeti FTB.

603 Maturity data from the subsurface of the Kura Basin are available only for the Maikop series and
604 indicate an immature to early mature stage of HC generation (Fig. 6) acquired during progressive

burial by the Middle-Late Miocene stratigraphic section (Pupp et al., 2018). Surface samples within the Kura Basin are also characterised by a low maturity level (Fig. 5), with maximum paleotemperatures in the 60-80°C range. Assuming 25-30°C/km as average geothermal gradient no more than 2-3 km of basin fill could have been eroded in the deformed Kura Basin. The low maturity of both surface and subsurface samples indicates a cold thermal regime, typical of flexural foreland basins (Fig. 8).

In the Kakheta ridge thermal maturity changes from the early mature to the immature stage of HC generation from the Lower Cretaceous to the Maikop sections, respectively, suggesting that maturity was acquired, as in the Kura Basin, as a consequence of sedimentary burial in a quite cold regime, with limited overthrusting effects on the organic matter indicators, whereas thrust-related fluid circulation may have affected clay mineralogy results (see Section 4.5). The Kakheta ridge was exhumed earlier than the rest of the Kura Basin (Fig. 10) and maturity is generally lower than in the wells drilled to the south of the ridge in the eastern and southern surroundings of Tbilisi, because of the lower amount of burial experienced. Our results indicate maximum paleotemperatures between 40 and 110°C, which roughly translate into 1-3.5 km of eroded basin fill (assuming 25-30°C/km of geothermal gradient).

The comparison of the thermal maturity distribution in the Adjara-Trialeti FTB (in its Paleocene-Miocene section), the Kura Basin (in its Oligocene-Miocene section) and the Kakheta ridge (in its Upper Cretaceous-Oligocene section), indicates that:

- Thermal maturity trends in the Adjara-Trialeti FTB and in the Kura Basin/Kakheta ridge are similar, showing an increase in maturity, from younger to older units, from immature to mid-mature oil window. The thickness of the Paleocene-Oligocene sections in the two domains is however different (i.e. 2-3 km thicker in the Adjara-Trialeti FTB), supporting the hypothesis that the final cumulative thermal maturity cannot be due to the same burial/thermal evolution through time. As recognized by Pupp et al. (2018), the maturation of the Oligocene-Lower Miocene source rock in

the Kura Basin in the Tbilisi area is due to sedimentation and tectonic thickening of the Neogene basin fill (Nemčok et al., 2013), thus acquired later than in the Adjara-Trialeti inverted basin.

- Peak temperatures in the Adjara-Trialeti basin must have been reached during back-arc basin evolution, probably due to enhanced sediment accumulation driven by subsidence in Paleocene-Early Miocene times when the Kura Basin substratum represented a relative structural high. This is also an indirect proof that in Middle-Late Miocene times the Adjara-Trialeti domain was no longer undergoing subsidence and was being exhumed. At the same time the adjacent Kura Basin was experiencing strong subsidence and sedimentation. This is supported by independent thermochronological data and models (Gusmeo et al., 2021) which define the onset of exhumation in the Adjara-Trialeti FTB at around 14-12 Ma.

- Compared with the Adjara-Trialeti FTB and the rest of the Kura Basin, the Kakhети ridge shows a slightly lower maturity in time-equivalent stratigraphic units (immature stage in the Oligocene section), confirming that pre-Middle Miocene burial did not cause significant maturation of the Maikop section. Furthermore, in Middle-Late Miocene times the fold-and-thrust belt shortened and started exhuming, with scarce accumulation of syn-tectonic sediments, confined in shallow thrust-top basins, later on sutured by Plio-Pleistocene sediments (Fig. 10a; Alania et al., 2017).

The highest paleotemperatures were recorded in the Greater Caucasus, with thermal maturity values spanning from the upper oil/gas generation window up to 200-250°C in the youngest units (the Upper Cretaceous-Eocene section at the front of the belt), to anchizone and epizone in the Jurassic section in the inner portion of the chain, where recorded maximum paleotemperatures exceed 300°C. Presently there are no constraints on the timing of acquisition of such a thermal signature; further work has still to be done in order to solve this issue.

These paleotemperatures, if we tentatively assume an average geothermal gradient of 25/30°C, suggest that a minimum of 3.5 km of basin fill has been removed in the southern foothills of the

Greater Caucasus, and up to 12.5 km of section may have been removed in the axial zone. These rough estimates are broadly in agreement with reconstructions of the total basin fill of the former Greater Caucasus Basin, although a contribution due to tectonic nappe emplacement to thermal maturity cannot be excluded (Adamia et al., 2011b; Saintot et al., 2006; Vincent et al., 2016).

Time-equivalent lithostratigraphic units in the Kakheti ridge and the Greater Caucasus (e.g., Oligocene-Late Eocene) underwent a different thermal evolution, suggesting that the Kakheti ridge, though appearing laterally contiguous with the southern Greater Caucasus orogenic edifice (Figs. 1 and 11), is not really akin to it. Thermal maturity trends in this fold-and-thrust belt are much more similar to the ones in the Kura Basin, thus confirming that the Kakheti ridge represents a highly tectonised and more deeply exhumed portion of that basin.

5.2 Regional geological evolution

In conclusion, the geological evolution of the sector comprised between the Adjara-Trialeti FTB and the Greater Caucasus can be described as follows (Fig. 11).

In the Late Eocene, both Adjara-Trialeti and Greater Caucasus basins were experiencing extensional subsidence, but with different degrees of extension and thickness of sedimentary fill. The Greater Caucasus Basin was characterized by a thin and intruded continental crust in its axial zone, and by a sedimentary succession at least 7-9 km thick (Adamia et al., 2011a, 2011b; Ershov et al., 2003; Saintot et al., 2006). The Adjara-Trialeti Basin was underlain by a thicker and less intruded continental crust and filled by a thinner sedimentary succession (with thickness variable along-strike) (Adamia et al., 2011b, 2017; Gamkrelidze et al., 2019; Nemčok et al., 2013; Okrostsvaridze et al., 2018; Yılmaz et al., 2000, 2014). Between the two basins, a structural high was located, characterized by a very thin sedimentary succession overlying the basement: this

structural high will later crop out as the Dzirula Massif, and more to the east it will represent the basement upon which the Kura Basin and the Kakheta ridge will develop.

The present-day situation witnesses both former basins closed and shortened through positive inversion, with the Kura Basin and the Kakheta ridge trapped between them. Growth of the Adjara-Trialeti FTB started in the late Middle Miocene (Gusmeo et al., 2021), while timing of Greater Caucasus growth is still debated (see section 2; Avdeev and Niemi, 2011; Forte et al., 2014; Vasey et al., 2020; Vincent et al., 2011, 2020). These two orogens are underlain by a thick continental crust, 35 to 45 km below the Adjara-Trialeti belt and 50-55 km in the Greater Caucasus (Adamia et al., 2017; Brunet et al., 2003; Ershov et al., 2003; Motavalli-Anbaran et al., 2016). The Kura Basin was flexured during convergence, mainly in Miocene times, when a thick pile of sedimentary rocks eroded from both the adjacent orogenic belts was deposited within the basin (Adamia et al., 2010; Pupp et al., 2018), causing maturation of the Maikop series, as evidenced in this study. The Maikop succession in the Kakheta ridge is characterised by a slightly lower maturity degree because the ridge was experiencing shortening and exhumation while the Kura Basin was still experiencing flexural subsidence and sedimentary burial.

Our thermal maturity results, integrated with published ones and with the structural framework of the study area, can be interpreted in the broader context of the Arabia-Eurasia collision zone. The tectonic evolution reconstructed in this paper, schematically summarised in Fig. 11 and derived from our thermal maturity data and independent stratigraphic and structural constraints, describes a net change in the dominant stress field which occurred in Middle Miocene times, when extensional tectonics was replaced by compression and the Adjara-Trialeti basin was structurally inverted (Alania et al., 2017; Forte et al., 2014; Gusmeo et al., 2021; Sukhishvili et al., 2020; Tari et al., 2018). Miocene shortening occurred also in the Greater Caucasus, although the timing of its inception is a matter of debate (Cowgill et al., 2016; Vasey et al., 2020; Vincent et al., 2020). This compressional geodynamic regime continues to the present day (Reilinger et al., 2006; Sokhadze et al., 2018; Tibaldi et al., 2019).

Inception of compressional tectonics in the study area is coeval with the Arabia-Eurasia hard collision along the Bitlis-Zagros suture zone (Cavazza et al., 2018; Okay et al., 2010). At the same time, wide areas of the suture-zone hinterland, comprising segments of the eastern Pontides, the Caucasus *s.l.*, the Talysh belt, and the Alborz range, were also subjected to deformation (Albino et al., 2014; Axen et al., 2001; Ballato et al., 2011, 2016; Cavazza et al., 2017, 2019; Gavillot et al., 2010; Gusmeo et al., 2021; Koshnaw et al., 2017, 2020; Madanipour et al., 2017; Su and Zhou, 2020; Tibaldi et al., 2017). From this viewpoint, the results shown in this paper further support the hypothesis that the compressional stresses associated to the Arabia-Eurasia hard collision might have been transmitted to the north over long distances, causing far-field deformation in a wide area of the hinterland.

A fundamental unresolved issue is the exact timing of growth and structural evolution of the Greater Caucasus, which according to our results has recorded a range of paleotemperatures much higher than those recorded in the other domains. The high maturity level in the axial zone of the belt and in the Jurassic-Cretaceous stratigraphic successions, characterised by a thick-skinned tectonic style, can be ascribed with confidence mostly to sedimentary burial. Middle Jurassic magmatic activity (Adamia et al., 2011a; Saintot et al., 2006) may have in part contributed to the very high paleotemperatures recorded in the oldest, most mature samples. Both the maturity trend and the structural style of deformation are in agreement with a positive inversion of the former extensional faults (similarly to the Adjara-Trialeti FTB). The fairly high paleotemperatures (100-160°C) experienced by the Upper Eocene succession of the Greater Caucasus southern foothills require a different explanation. Such maturity level can result from either (i) sedimentary burial underneath a thick succession of younger sedimentary rocks, later almost totally eroded, or (ii) thrust-related tectonic burial. The discrimination of the dominant contribution (sedimentary, tectonic, or both) to the thermal maturity of this part of the belt has crucial implications for a precise reconstruction of the Cenozoic development of the Greater Caucasus.

6. Conclusions

This paper provides new constraints on the thermal evolution and the structural styles of a wide area in eastern Georgia, where three geologic domains can be identified in the hinterland of the Arabia-Eurasia collision zone. Two domains derived from positive inversion of former rift basins (i.e. Adjara-Trialeti FTB and Greater Caucasus), the third is comprised between them and characterised by thin-skinned deformation (i.e. Kura Basin and Kakheti ridge). Integrating newly acquired and published thermal maturity indicators we were able to (i) define the maximum temperatures experienced by the sedimentary successions and (ii) to elucidate the tectonic evolution of the area of study during convergence, including the role played by inherited pre-shortening structures.

The results indicate that the Cretaceous-to-Lower Miocene sedimentary units in the Adjara-Trialeti FTB and in the Kura Basin have a similar thermal maturity degree, comprised in the oil window, whereas time-equivalent successions in the Kakheti ridge are slightly less mature (immature to early mature) and the Middle-Late Miocene section of the Kura Basin is immature. The similar thermal maturity in the same stratigraphic units was acquired during back-arc basin evolution in the Paleogene in the Adjara-Trialeti FTB, and during flexure and sedimentary burial, associated to convergence, in the Miocene in the Kura Basin/Kakheti ridge. The Greater Caucasus is characterised by a much higher maturity level, increasing from the southern foothills to the axial zone, where it reaches the low metamorphic realm. Such a maturity probably represents the cumulative effect of both sedimentary burial during extensional evolution and tectonic overburden during compressional deformation.

Acknowledgements

Organic petrography and XRD analyses of fine-grained sediments were performed in ALBA (Academic Laboratory of Basin Analysis) of the Department of Science of “Roma Tre” University. Raman analyses and interpretation have been performed in EVPL (Experimental Volcanology and Petrology Laboratory) of the Department of Science of “Roma Tre” University. Pyrolysis data were kindly provided by Georgia Oil and Gas Company.

Warm acknowledgments to Sergio Lo Mastro for XRD diffractogram acquisition.

Tamar Beridze and Luca Aldega are warmly acknowledged for fruitful discussions on Georgia regional geology and thermal evolution of sedimentary basins.

Constructive comments made by Jocelyn Barbarand and Gabor Tari improved an earlier version of the manuscript. We also thank Associate Editor Johannes Wendebourg for careful handling of the manuscript.

Funding: MUR-PRIN 2017-2021; MUR-Department of Excellence Science Roma Tre; Roma Tre Post-doc grant to A. Schito; ALBA Laboratory funds; MUR PhD grant to T. Gusmeo. Funding sources only provided financial support and did not in any way influence the study design, data interpretation, the writing process or the decision to submit this manuscript.

References

- Adamia, S.A., 2004. Geological Map of Georgia, 1: 500 000 scale.
- Adamia, S.A., Alania, V., Chabukiani, A., Chichua, G., Enukidze, O., Sadradze, N., 2010. Evolution of the Late Cenozoic basins of Georgia (SW Caucasus): a review, in: Sosson, M., Kaymakci, N., Stephenson, R.A., Bergerat, F., Starostenko, V. (Eds.), *Sedimentary Basin Tectonics from the Black Sea and Caucasus to the Arabian Platform*. Geological Society, London, Special Publications, 340, pp. 239–259.
- Adamia, S.A., Alania, V., Chabukiani, A., Kutelia, Z., Sadradze, N., 2011a. Great Caucasus (Cavcasioni): A Long-lived North-Tethyan Back-Arc Basin. *Turkish J. Earth Sci.* 20, 611–628.

780 <https://doi.org/10.3906/yer-1005-12>

781 Adamia, S.A., Chkhotua, T., Kekelia, M., Lordkipanidze, M., Shavishvili, I., Zakariadze, G., 1981.
782 Tectonics of the Caucasus and adjoining regions: implications for the evolution of the Tethys
783 ocean. *J. Struct. Geol.* 3, 437–447. [https://doi.org/10.1016/0191-](https://doi.org/10.1016/0191-8141(81)90043-2)
784 8141(81)90043-2

785 Adamia, S.A., Chkhotua, T.G., Gavtadze, T.T., Lebanidze, Z.A., Lursmanashvili, N.D., Sadradze,
786 N.G., Zakaraia, D.P., Zakariadze, G.S., 2017. Tectonic setting of Georgia-Eastern Black Sea:
787 A review, in: Sosson, M., Stephenson, R.A., Adamia, S.A. (Eds.), *Tectonic Evolution of the*
788 *Eastern Black Sea and Caucasus*. Geological Society, London, Special Publications 428, pp.
789 11–40. <https://doi.org/10.1144/SP428.6>

790 Adamia, S.A., Zakariadze, G., Chkhotua, T., Sadradze, N., Tsereteli, N., Chabukiani, A.,
791 Gventsadze, A., 2011b. Geology of the Caucasus: A Review. *Turkish J. Earth Sci.* 20, 489–
792 544. <https://doi.org/10.3906/yer-1005-11>

793 Alania, V., Beridze, T., Enukidze, O., Chagelishvili, R., Lebanidze, Z., Maqadze, D., 2021. The
794 Geometry of the two orogens convergence and collision zones in central Georgia: new data
795 from seismic reflection profiles, in: Bonali, F.L., Pasquarè Mariotto, F.A., Tsereteli, N. (Eds.),
796 *Building Knowledge for Geohazard Assessment and Management in the Caucasus and Other*
797 *Regions*. Springer, Dordrecht, pp. 73–88.

798 Alania, V., Beridze, T., Enukidze, O., Lebanidze, Z., Razmadze, A., Sadradze, N., Tevzadze, N.,
799 2020. Structural model of the frontal part of the eastern Achara-Trialeti fold-and-thrust belt:
800 The results of seismic profile interpretation. *Bull. Georg. Natl. Acad. Sci.* 14, 62–68.

801 Alania, V., Chabukiani, A.O., Chagelishvili, R.L., Enukidze, O. V., Gogrichiani, K.O., Razmadze,
802 A.N., Tsereteli, N.S., 2017. Growth structures, piggy-back basins and growth strata of the
803 Georgian part of the Kura foreland fold–thrust belt: implications for Late Alpine kinematic
804 evolution, in: Sosson, M., Stephenson, R.A., Adamia, S.A. (Eds.), *Tectonic Evolution of the*

- 805 Eastern Black Sea and Caucasus. Geological Society, London, Special Publications 428, pp.
 806 428–445. <https://doi.org/10.1177/1010539510370992>
- 807 Alania, V., Enukidze, O., Glonti, N., Razmadze, A., Chabukiani, A., Giorgadze, A., Vakhtang
 808 Glonti, B., Koiava, K., Beridze, T., Khutsishvili, S., Chagelishvili, R., 2018. Structural
 809 Architecture of the Kura Foreland Fold-and-thrust Belt Using Seismic Reflection Profile,
 810 Georgia. *Univers. J. Geosci.* 6, 184–190. <https://doi.org/10.13189/ujg.2018.060402>
- 811 Albino, I., Cavazza, W., Zattin, M., Okay, A.I., Adamia, S.A., Sadradze, N., 2014. Far-field
 812 tectonic effects of the Arabia–Eurasia collision and the inception of the North Anatolian Fault
 813 system. *Geol. Mag.* 151, 372–379. <https://doi.org/10.1017/s0016756813000952>
- 814 Aldega, L., Bigi, S., Carminati, E., Trippetta, F., Corrado, S., Kavooosi, M.A., 2018. The Zagros
 815 fold-and-thrust belt in the Fars province (Iran): II. Thermal evolution. *Mar. Pet. Geol.* 93, 376–
 816 390. <https://doi.org/10.1016/j.marpetgeo.2018.03.022>
- 817 Aldega, L., Botti, F., Corrado, S., 2007a. Clay mineral assemblages and vitrinite reflectance in the
 818 Laga Basin (Central Apennines, Italy): What do they record? *Clays Clay Miner.* 55, 504–518.
 819 <https://doi.org/10.1346/CCMN.2007.0550505>
- 820 Aldega, L., Corrado, S., Carminati, E., Shaban, A., Sherkati, S., 2014. Thermal evolution of the
 821 Kuh-e-Asmari and Sim anticlines in the Zagros fold-and-thrust belt: Implications for
 822 hydrocarbon generation. *Mar. Pet. Geol.* 57, 1–13.
 823 <https://doi.org/10.1016/j.marpetgeo.2014.04.017>
- 824 Aldega, L., Corrado, S., Grasso, M., Maniscalco, R., 2007b. Correlation of Diagenetic Data from
 825 Organic and Inorganic Studies in the Apenninic- Maghrebian Fold- and- Thrust Belt: A Case
 826 Study from Eastern Sicily. *J. Geol.* 115, 335–353. <https://doi.org/10.1086/512756>
- 827 Aldega, L., Corrado, S., Paolo, L. Di, Somma, R., Maniscalco, R., Balestrieri, M.L., 2011. Shallow
 828 burial and exhumation of the Peloritani Mountains (NE Sicily, Italy): Insight from

- 829 paleothermal and structural indicators. *Bull. Geol. Soc. Am.* 123, 132–149.
 830 <https://doi.org/10.1130/B30093.1>
- 831 Allen, P.A., Allen, J.R., 2013. *Basin Analysis: Principles and Application to Petroleum Play*
 832 *Assessment, Science*. <https://doi.org/10.1126/science.208.4442.393>
- 833 Atouabat, A., Corrado, S., Schito, A., Haissen, F., Gimeno-Vives, O., Mohn, G., Lamotte, D.F. de,
 834 2020. Validating structural styles in the Flysch Basin Northern Rif (Morocco) by means of
 835 thermal modeling. *Geosci.* 10, 1–18. <https://doi.org/10.3390/geosciences10090325>
- 836 Avdeev, B., Niemi, N.A., 2011. Rapid Pliocene exhumation of the central Greater Caucasus
 837 constrained by low-temperature thermochronometry. *Tectonics* 30, 1–16.
 838 <https://doi.org/10.1029/2010TC002808>
- 839 Axen, G.J., Lam, P.S., Grove, M., Stockli, D.F., Hassanzadeh, J., 2001. Exhumation of the west-
 840 central Alborz Mountains, Iran, Caspian subsidence, and collision-related tectonics. *Geology*
 841 29, 559–562. [https://doi.org/10.1130/0091-7613\(2001\)029<0559:EOTWCA>2.0.CO;2](https://doi.org/10.1130/0091-7613(2001)029<0559:EOTWCA>2.0.CO;2)
- 842 Balestra, M., Corrado, S., Aldega, L., Morticelli, M.G., Sulli, A., Rudkiewicz, J.L., Sassi, W., 2019.
 843 Thermal and structural modeling of the Scillato wedge-top basin source-to-sink system:
 844 Insights into the Sicilian fold-and-thrust belt evolution (Italy). *Bull. Geol. Soc. Am.* 131,
 845 1763–1782. <https://doi.org/10.1130/B35078.1>
- 846 Ballato, P., Cifelli, F., Heidarzadeh, G., Ghassemi, M.R., Wickert, A.D., Hassanzadeh, J., Dupont-
 847 Nivet, G., Balling, P., Sudo, M., Zeilinger, G., Schmitt, A.K., Mattei, M., Strecker, M.R.,
 848 2016. Tectono-sedimentary evolution of the northern Iranian Plateau: insights from middle-
 849 late Miocene foreland-basin deposits. *Basin Res.* 29, 417–446.
 850 <https://doi.org/10.1111/bre.12180>
- 851 Ballato, P., Uba, C.E., Landgraf, A., Strecker, M.R., Sudo, M., Stockli, D.F., Friedrich, A.,
 852 Tabatabaei, S.H., 2011. Arabia-Eurasia continental collision: Insights from late Tertiary

- 853 foreland-basin evolution in the Alborz Mountains, Northern Iran. *Bull. Geol. Soc. Am.* 123,
854 106–131. <https://doi.org/10.1130/B30091.1>
- 855 Banks, C.J., Robinson, A.G., Williams, M.P., 1997. Structure and regional tectonics of the Achara-
856 Trialeti fold belt and the adjacent Rioni and Kartli foreland basins, Republic of Georgia, in:
857 Robinson, A.G. (Ed.), *Regional and Petroleum Geology of the Black Sea and Surrounding*
858 *Region: AAPG Memoirs 68*. Tulsa, Oklahoma, pp. 331–346.
- 859 Barker, C.E., Pawlewicz, M.J., 1986. The correlation of vitrinite reflectance with maximum
860 temperature in humic organic matter, in: Buntebarth, G., Stagena, L. (Eds.), *Paleogeothermics*.
861 Springer, Berlin, Heidelberg, pp. 79–93. [https://doi.org/https://doi.org/10.1007/BFb0012103](https://doi.org/10.1007/BFb0012103)
- 862 Barnard, P.C., Collins, A.G., Cooper, B.S., 1981. Identification and distribution of kerogen facies in
863 a source rock horizon - examples from the North Sea Basin., in: Brooks, J. (Ed.), *Organic*
864 *Maturation Studies and Fossil Fuel Exploration*. Academic Press, London, pp. 271–282.
- 865 Barnes, M.A., Barnes, W.C., Bustin, R.M., 1990. Chemistry and diagenesis of organic matter in
866 sediments and fossil fuels. *Diagenesis* 189–204.
- 867 Barrier, E., Vrielynck, B., Brouillet, J.F., Brunet, M.-F., (Contributors: Angiolini L., Kaveh F.,
868 Poisson A., Pourteau A., Plunder A., Robertson A., Shekawat R., Sosson M., Zanchi, A.),
869 2018. Paleotectonic reconstruction of the central Tethyan realm. *Tectono-sedimentary-*
870 *palinspastic maps from late Permian to Pliocene*. CCGM/CGMW, Paris.
- 871 Behar, F., Beaumont, V., De B. Pentead, H.L., 2001. Rock-Eval 6 Technology: Performances and
872 Developments. *Oil Gas Sci. Technol.* 56, 111–134. <https://doi.org/10.2516/ogst:2001013>
- 873 Bertrand, R., Lavoie, V., Malo, M., 2010. Maturité thermique et potentiel roche-mère des roches
874 ordoviciennes à dévoniennes du secteur Matapédia–Témiscouata du Bas-Saint-Laurent,
875 Québec. *Geol. Surv. Canada, Open File 6576* 183.
- 876 Beyssac, O., Goffe, B., Chopin, C., Rouzaud, J.N., 2002. Raman spectra of carbonaceous material

- 877 in metasediments: a new geothermometer. *J. Metamorph. Geol.* *J Metamorph Geol* 20, 859–
878 871.
- 879 Boote, D.R.D., Sachsenhofer, R.F., Tari, G., Arbouille, D., 2018. Petroleum Provinces of the
880 Paratethyan Region. *J. Pet. Geol.* 41, 247–298. <https://doi.org/10.1111/jpg.12703>
- 881 Borrego, A.G., Araujo, C. V., Balke, A., Cardott, B., Cook, A.C., David, P., Flores, D., Hámor-
882 Vidó, M., Hiltmann, W., Kalkreuth, W., Koch, J., Kommeren, C.J., Kus, J., Ligouis, B.,
883 Marques, M., Mendonça Filho, J.G., Misz, M., Oliveira, L., Pickel, W., Reimer, K.,
884 Ranasinghe, P., Suárez-Ruiz, I., Vieth, A., 2006. Influence of particle and surface quality on
885 the vitrinite reflectance of dispersed organic matter: Comparative exercise using data from the
886 qualifying system for reflectance analysis working group of ICCP. *Int. J. Coal Geol.* 68, 151–
887 170. <https://doi.org/10.1016/j.coal.2006.02.002>
- 888 Borrego, A.G., Cook, A., 2017. Sampling and Sample Preparation for Reflected Light Microscopy,
889 in: 10th ICCP Training Course on Dispersed Organic Matter Integrating Transmitted and
890 Reflected Light Microscopy (Instruction Notes). pp. 21–28.
- 891 Brunet, F.F., Korotaev, M. V., Ershov, A. V., Nikishin, A.M., 2003. The South Caspian Basin: A
892 review of its evolution from subsidence modelling. *Sediment. Geol.* 156, 119–148.
893 [https://doi.org/10.1016/S0037-0738\(02\)00285-3](https://doi.org/10.1016/S0037-0738(02)00285-3)
- 894 Bujakaite, M.I., Gavrilov, Y.O., Gertsev, D.O., Golovin, D.I., Panov, D.I., Kushcheva, Y. V., 2003.
895 The K–Ar and Rb–Sr Isotopic Systems in Rocks from the Jurassic Terrigenous Complex of the
896 Greater Caucasus. *Lithol. Miner. Resour.* 38, 522–529.
897 <https://doi.org/10.1023/A:1027364527305>
- 898 Burnham, A.K., Sweeney, J.J., 1989. A chemical kinetic model of vitrinite maturation and
899 reflectance. *Geochim. Cosmochim. Acta* 53, 2649–2657. [https://doi.org/10.1016/0016-](https://doi.org/10.1016/0016-7037(89)90136-1)
900 [7037\(89\)90136-1](https://doi.org/10.1016/0016-7037(89)90136-1)

- 901 Caricchi, C., Aldega, L., Corrado, S., 2015. Reconstruction of maximum burial along the Northern
 902 Apennines thrust wedge (Italy) by indicators of thermal exposure and modeling. *Bull. Geol.*
 903 *Soc. Am.* 127, 428–442. <https://doi.org/10.1130/B30947.1>
- 904 Cavazza, W., Albino, I., Galoyan, G., Zattin, M., Cattò, S., 2019. Continental accretion and
 905 incremental deformation in the thermochronologic evolution of the Lesser Caucasus. *Geosci.*
 906 *Front.* <https://doi.org/10.1016/j.gsf.2019.02.007>
- 907 Cavazza, W., Albino, I., Zattin, M., Galoyan, G., Imamverdiyev, N., Melkonyan, R., 2017.
 908 Thermochronometric evidence for Miocene tectonic reactivation of the Sevan-Akera suture
 909 zone (Lesser Caucasus): A far-field tectonic effect of the Arabia-Eurasia collision?, in: Sosson,
 910 M., Stephenson, R.A., Adamia, S.A. (Eds.), *Tectonic Evolution of the Eastern Black Sea and*
 911 *Caucasus*. Geological Society, London, Special Publications 428, pp. 187–198.
 912 <https://doi.org/10.1144/SP428.4>
- 913 Cavazza, W., Cattò, S., Zattin, M., Okay, A.I., Reiners, P., 2018. Thermochronology of the
 914 Miocene Arabia-Eurasia collision zone of southeastern Turkey. *Geosphere* 14, 2277–2293.
 915 <https://doi.org/10.1130/GES01637.1>
- 916 Corrado, S., Aldega, L., Balestrieri, M.L., Maniscalco, R., Grasso, M., 2009. Structural evolution of
 917 the sedimentary accretionary wedge of the alpine system in Eastern Sicily: Thermal and
 918 thermochronological constraints. *Bull. Geol. Soc. Am.* 121, 1475–1490.
 919 <https://doi.org/10.1130/B26420.1>
- 920 Corrado, S., Aldega, L., Di Leo, P., Giampaolo, C., Invernizzi, C., Mazzoli, S., Zattin, M., 2005.
 921 Thermal maturity of the axial zone of the southern Apennines fold-and-thrust belt (Italy) from
 922 multiple organic and inorganic indicators. *Terra Nov.* 17, 56–65.
 923 <https://doi.org/10.1111/j.1365-3121.2004.00584.x>
- 924 Corrado, S., Schito, A., Romano, C., Grigo, D., Poe, B.T., Aldega, L., Caricchi, C., Di Paolo, L.,
 925 Zattin, M., 2020. An integrated platform for thermal maturity assessment of polyphase, long-

- 926 lasting sedimentary basins, from classical to brand-new thermal parameters and models: An
 927 example from the on-shore Baltic Basin (Poland). *Mar. Pet. Geol.* 122, 104547.
 928 <https://doi.org/10.1016/j.marpetgeo.2020.104547>
- 929 Cowgill, E., Forte, A.M., Niemi, N., Avdeev, B., Tye, A., Trexler, C., Javakhishvili, Z., Elashvili,
 930 M., Godoladze, T., 2016. Relict basin closure and crustal shortening budgets during
 931 continental collision: An example from Caucasus sediment provenance. *Tectonics* 35, 2918–
 932 2947. <https://doi.org/10.1002/2016TC004295>
- 933 Dercourt, J., Zonenshain, L.P., Ricou, L.E., Kazmin, V.G., Le Pichon, X., Knipper, A.L.,
 934 Grandjacquet, C., Sbertshikov, I.M., Geyssant, J., Lepvrier, C., Pechersky, D.H., Boulin, J.,
 935 Sibuet, J.C., Savostin, L.A., Sorokhtin, O., Westphal, M., Bazhenov, M.L., Lauer, J.P., Bijou-
 936 Duval, B., 1986. Geological evolution of the Tethys belt from the Atlantic to the Pamirs since
 937 the Lias. *Tectonophysics* 123, 241–315. [https://doi.org/10.1016/0040-1951\(86\)90199-X](https://doi.org/10.1016/0040-1951(86)90199-X)
- 938 Di Paolo, L., Olivetti, V., Corrado, S., Aldega, L., Balestrieri, M.L., Maniscalco, R., 2014.
 939 Detecting the stepwise propagation of the Eastern Sicily thrust belt (Italy): Insight from
 940 thermal and thermochronological constraints. *Terra Nov.* 26, 363–371.
 941 <https://doi.org/10.1111/ter.12106>
- 942 Dow, W.G., 1977. Kerogen studies and geological interpretations. *J. Geochemical Explor.* 7, 79–99.
- 943 Ershov, A. V., Brunet, M.F., Nikishin, A.M., Bolotov, S.N., Nazarevich, B.P., Korotaev, M. V.,
 944 2003. Northern Caucasus basin: Thermal history and synthesis of subsidence models.
 945 *Sediment. Geol.* 156, 95–118. [https://doi.org/10.1016/S0037-0738\(02\)00284-1](https://doi.org/10.1016/S0037-0738(02)00284-1)
- 946 Ferralis, N., Matys, E.D., Knoll, A.H., Hallmann, C., Summons, R.E., 2016. Rapid, direct and non-
 947 destructive assessment of fossil organic matter via microRaman spectroscopy. *Carbon N. Y.*
 948 108, 440–449. <https://doi.org/10.1016/j.carbon.2016.07.039>
- 949 Forte, A.M., Cowgill, E., Bernardin, T., Kreylos, O., Hamann, B., 2010. Late Cenozoic deformation

- 950 of the Kura fold-thrust belt, southern Greater Caucasus. *Bull. Geol. Soc. Am.* 122, 465–486.
 951 <https://doi.org/10.1130/B26464.1>
- 952 Forte, A.M., Cowgill, E., Murtuzayev, I., Kangarli, T., Stoica, M., 2013. Structural geometries and
 953 magnitude of shortening in the eastern Kura fold-thrust belt, Azerbaijan: Implications for the
 954 development of the Greater Caucasus Mountains. *Tectonics* 32, 688–717.
 955 <https://doi.org/10.1002/tect.20032>
- 956 Forte, A.M., Cowgill, E., Whipple, K.X., 2014. Transition from a singly vergent to doubly vergent
 957 wedge in a young orogen: The Greater Caucasus. *Tectonics* 33, 2077–2101.
 958 <https://doi.org/10.1002/2014TC003651>
- 959 Gamkrelidze, I., Okrostsvaridze, A., Maisadze, F., Basheleishvili, L., Boichenko, G., 2019. Main
 960 features of geological structure and geotourism potential of Georgia, the Caucasus. *Mod.*
 961 *Environ. Sci. Eng.* 5, 422–442. [https://doi.org/10.15341/mese\(2333-2581\)/05.05.2019/010](https://doi.org/10.15341/mese(2333-2581)/05.05.2019/010)
- 962 Gavillot, Y., Axen, G.J., Stockli, D.F., Horton, B.K., Fakhari, M.D., 2010. Timing of thrust activity
 963 in the High Zagros fold-thrust belt, Iran, from (U-Th)/He thermochronometry. *Tectonics* 29.
 964 <https://doi.org/10.1029/2009TC002484>
- 965 Goodhue, R., Clayton, G., 2010. Palynomorph darkness index (PDI) - A new technique for
 966 assessing thermal maturity. *Palynology* 34, 147–156.
 967 <https://doi.org/10.1080/01916121003696932>
- 968 Guedes, A., Valentim, B., Prieto, A.C., Noronha, F., 2012. Raman spectroscopy of coal macerals
 969 and fluidized bed char morphotypes. *Fuel* 97, 443–449.
 970 <https://doi.org/10.1016/j.fuel.2012.02.054>
- 971 Guedes, A., Valentim, B., Prieto, A.C., Rodrigues, S., Noronha, F., 2010. Micro-Raman
 972 spectroscopy of collotelinite, fusinite and macrinite. *Int. J. Coal Geol.* 83, 415–422.
 973 <https://doi.org/10.1016/j.coal.2010.06.002>

- 974 Gusmeo, T., Cavazza, W., Alania, V.M., Enukidze, O. V, Zattin, M., Corrado, S., 2021. Structural
 975 inversion of back-arc basins – The Neogene Adjara-Trialeti fold-and-thrust belt (SW Georgia)
 976 as a far-field effect of the Arabia-Eurasia collision. *Tectonophysics* 803.
 977 <https://doi.org/10.1016/j.tecto.2020.228702>
- 978 Hartkopf-Fröder, C., Königshof, P., Littke, R., Schwarzbauer, J., 2015. Optical thermal maturity
 979 parameters and organic geochemical alteration at low grade diagenesis to anchimetamorphism:
 980 A review. *Int. J. Coal Geol.* 150–151, 74–119. <https://doi.org/10.1016/j.coal.2015.06.005>
- 981 Henry, D.G., Jarvis, I., Gillmore, G., Stephenson, M., 2019. Raman spectroscopy as a tool to
 982 determine the thermal maturity of organic matter: Application to sedimentary, metamorphic
 983 and structural geology. *Earth-Science Rev.* 198, 102936.
 984 <https://doi.org/10.1016/j.earscirev.2019.102936>
- 985 Hillier, S., Mátyás, J., Matter, A., Vasseur, G., 1995. Illite/Smectite Diagenesis and Its Variable
 986 Correlation with Vitrinite Reflectance in the Pannonian Basin. *Clays Clay Miner.* 43, 174–183.
- 987 Hinrichs, R., Brown, M.T., Vasconcellos, M.A.Z., Abrashev, M. V., Kalkreuth, W., 2014. Simple
 988 procedure for an estimation of the coal rank using micro-Raman spectroscopy. *Int. J. Coal*
 989 *Geol.* 136, 52–58. <https://doi.org/10.1016/j.coal.2014.10.013>
- 990 Hoffman, J., Hower, J., 1979. Clay mineral assemblages as low grade metamorphic
 991 geothermometers: application to the thrust faulted disturbed belt of Montana. *Soc. Econ.*
 992 *Plaeontologists Mineral.* 26, 55–79.
- 993 Jagodzinski, H., 1949. Eindimensionale Fehlordnung in Kristallen und ihr Einfluss auf die
 994 Röntgeninterferenzen. I. Berechnung des Fehlordnungsgrades aus den Röntgenintensitäten.
 995 *Acta Crystallogr.* 2, 201–207.
- 996 Koshnaw, R.I., Horton, B.K., Stockli, D.F., Barber, D.E., Tamar-Agha, M.Y., Kendall, J.J., 2017.
 997 Neogene shortening and exhumation of the Zagros fold-thrust belt and foreland basin in the

- 998 Kurdistan region of northern Iraq. *Tectonophysics* 694, 332–355.
 999 <https://doi.org/10.1016/j.tecto.2016.11.016>
- 1000 Koshnaw, R.I., Stockli, D.F., Horton, B.K., Teixell, A., Barber, D.E., Kendall, J.J., 2020. Late
 1001 Miocene deformation kinematics along the NW Zagros fold- thrust belt, Kurdistan region of
 1002 Iraq: Constraints from apatite (U- Th)/He thermochronometry and balanced cross sections.
 1003 *Tectonics* 1–37. <https://doi.org/10.1029/2019tc005865>
- 1004 Kübler, B., 1964. Les argilles, indicateurs de métamorphisme. *Rev. l’Institut Fr. du Pet.* 19, 1093–
 1005 1112.
- 1006 Kübler, B., Jaboyedoff, M., 2000. Illite crystallinity. *Comptes Rendus l’Academie Sci. - Ser. Ila*
 1007 *Sci. la Terre des Planetes* 331, 75–89. [https://doi.org/10.1016/S1251-8050\(00\)01395-1](https://doi.org/10.1016/S1251-8050(00)01395-1)
- 1008 Labeur, A., Beaudoin, N.E., Lacombe, O., Emmanuel, L., Petracchini, L., Daëron, M., Klimowicz,
 1009 S., Callot, J.-P., 2021. Burial-deformation history of folded rocks unraveled by fracture
 1010 analysis, stylolite paleopiezometry and vein cement geochemistry: a case study in the Cingoli
 1011 Anticline (Umbria-Marche, Northern Appennines). *Geosciences* 11, 135–155.
 1012 <https://doi.org/10.3390/geosciences11030135>
- 1013 Lahfid, A., Beyssac, O., Deville, E., Negro, F., Chopin, C., Goffé, B., 2010. Evolution of the
 1014 Raman spectrum of carbonaceous material in low-grade metasediments of the Glarus Alps
 1015 (Switzerland). *Terra Nov.* 22, 354–360. <https://doi.org/10.1111/j.1365-3121.2010.00956.x>
- 1016 Lanson, B., 1997. Decomposition of experimental x-ray diffraction patterns (profile fitting): A
 1017 convenient way to study clay minerals. *Clays Clay Miner.* 45, 132–146.
 1018 <https://doi.org/10.1346/CCMN.1997.0450202>
- 1019 Lazarev, S., Jorissen, E.L., van de Velde, S., Rausch, L., Stoica, M., Wesselingh, F.P., Van Baak,
 1020 C.G.C., Yanina, T.A., Aliyeva, E., Krijgsman, W., 2019. Magneto-biostratigraphic age
 1021 constraints on the palaeoenvironmental evolution of the South Caspian basin during the Early-

- 1022 Middle Pleistocene (Kura basin, Azerbaijan). *Quat. Sci. Rev.* 222, 105895.
 1023 <https://doi.org/10.1016/j.quascirev.2019.105895>
- 1024 Liu, B., Schieber, J., Mastarletz, M., 2019. Petrographic and Micro-FTIR study of organic matter in
 1025 the Upper Devonian New Albany shale during thermal maturation: Implications for kerogen
 1026 transformation, in: Camp, W.K., Milliken, K.L., Taylor, K., Fishman, N., Hackley, P.C.,
 1027 Macquaker, J.H.S. (Eds.), *Mudstone Diagenesis: Research Perspectives for Shale Hydrocarbon*
 1028 *Reservoirs, Seals, and Source Rocks*. AAPG Memoir 120, pp. 165–188.
 1029 <https://doi.org/10.1306/13672216M1213380>
- 1030 Liu, D.H., Xiao, X.M., Tian, H., Min, Y.S., Zhou, Q., Cheng, P., Shen, J.G., 2013. Sample
 1031 maturation calculated using Raman spectroscopic parameters for solid organics: Methodology
 1032 and geological applications. *Chinese Sci. Bull.* 58, 1285–1298. [https://doi.org/10.1007/s11434-](https://doi.org/10.1007/s11434-012-5535-y)
 1033 [012-5535-y](https://doi.org/10.1007/s11434-012-5535-y)
- 1034 Lordkipanidze, M.B., Meliksetian, B., Djarbashian, R., 1989. Mesozoic-Cenozoic magmatic
 1035 evolution of the Pontian-Crimean-Caucasian region. *IGCP Proj.* 198 103–124.
- 1036 Lozar, F., Polino, R., 1997. Early Cenozoic uprising of the Great Caucasus revealed by reworked
 1037 calcareous nannofossils, in: *EUG. Strasbourg, France*, p. 141.
- 1038 Lünsdorf, N.K., Dunkl, I., Schmidt, B.C., Rantitsch, G., von Eynatten, H., 2017. Towards a Higher
 1039 Comparability of Geothermometric Data Obtained by Raman Spectroscopy of Carbonaceous
 1040 Material. Part 2: A Revised Geothermometer. *Geostand. Geoanalytical Res.* 41, 593–612.
 1041 <https://doi.org/10.1111/ggr.12178>
- 1042 Lünsdorf, N.K., Lünsdorf, J.O., 2016. Evaluating Raman spectra of carbonaceous matter by
 1043 automated, iterative curve-fitting. *Int. J. Coal Geol.* 160–161, 51–62.
 1044 <https://doi.org/10.1016/j.coal.2016.04.008>
- 1045 Madanipour, S., Ehlers, T.A., Yassaghi, A., Enkelmann, E., 2017. Accelerated middle Miocene

- 1046 exhumation of the Talesh Mountains constrained by U-Th/He thermochronometry: Evidence
 1047 for the Arabia-Eurasia collision in the NW Iranian Plateau. *Tectonics* 36, 1538–1561.
 1048 <https://doi.org/10.1002/2016TC004291>
- 1049 Mangenot, X., Bonifacie, M., Gasparrini, M., Götz, A., Chaduteau, C., Ader, M., Rouchon, V.,
 1050 2017. Coupling $\Delta 47$ and fluid inclusion thermometry on carbonate cements to precisely
 1051 reconstruct the temperature, salinity and $\delta 18\text{O}$ of paleo-groundwater in sedimentary basins.
 1052 *Chem. Geol.* 472, 44–57. <https://doi.org/10.1016/j.chemgeo.2017.10.011>
- 1053 Mangenot, X., Deçoninck, J.F., Bonifacie, M., Rouchon, V., Collin, P.Y., Quesne, D., Gasparrini,
 1054 M., Sizun, J.P., 2019. Thermal and exhumation histories of the northern subalpine chains
 1055 (Bauges and Bornes—France): Evidence from forward thermal modeling coupling clay
 1056 mineral diagenesis, organic maturity and carbonate clumped isotope ($\Delta 47$) data. *Basin Res.*
 1057 31, 361–379. <https://doi.org/10.1111/bre.12324>
- 1058 Mauvilly, J., Koiava, K., Gamkrelidze, I., Mosar, J., 2016. Tectonics in the Georgian Greater
 1059 Caucasus: a structural cross-section in an inverted rifted basin setting, in: 14th Swiss
 1060 Geoscience Meeting, Geneva, Switzerland. Geneva, Switzerland.
 1061 <https://doi.org/10.13140/RG.2.2.26540.56963>
- 1062 Merryman, R.J., Frey, M., 1999. Patterns of very low- grade metamorphism in metapelitic rocks,
 1063 in: *Low-Grade Metamorphism*. Blackwell Scientific Publications, Oxford, International, pp.
 1064 61–107.
- 1065 Moore, D.M., Reynolds, R.C.J., 1997. X-Ray Diffraction and the Identification and Analysis of
 1066 Clay Minerals. Oxford Univ Press. <https://doi.org/10.1180/claymin.1999.034.1.21>
- 1067 Mosar, J., Kangarli, T., Bochud, M., Glasmacher, U.A., Rast, A., Brunet, M.-F., Sosson, M., 2010.
 1068 Cenozoic-Recent tectonics and uplift in the Greater Caucasus: a perspective from Azerbaijan,
 1069 in: Sosson, M., Kaymakci, N., Stephenson, R.A., Bergerat, F., Starostenko, V. (Eds.),
 1070 *Sedimentary Basin Tectonics from the Black Sea and Caucasus to the Arabian Platform*.

- 1071 Geological Society, London, Special Publications 340, pp. 261–280.
 1072 <https://doi.org/10.1144/SP340.12>
- 1073 Motavalli-Anbaran, S.H., Zeyen, H., Jamasb, A., 2016. 3D crustal and lithospheric model of the
 1074 Arabia-Eurasia collision zone. *J. Asian Earth Sci.* 122, 158–167.
 1075 <https://doi.org/10.1016/j.jseaes.2016.03.012>
- 1076 Muirhead, D.K., Bond, C.E., Watkins, H., Butler, R.W.H., Schito, A., Crawford, Z., Marpino, A.,
 1077 2020. Raman Spectroscopy: an effective thermal marker in low temperature carbonaceous
 1078 fold-thrust belts, in: Hammerstein, J.A., Di Cuia, R., Cottam, M.A., Zamora, G., Butler,
 1079 R.W.H. (Eds.), *Fold and Thrust Belts: Structural Style, Evolution and Exploration*. Geological
 1080 Society, London, Special Publications 490, pp. 131–151. [https://doi.org/10.1144/SP490-2019-](https://doi.org/10.1144/SP490-2019-27)
 1081 [27](https://doi.org/10.1144/SP490-2019-27)
- 1082 Mumm, A.S., Inan, S., 2016. Microscale organic maturity determination of graptolites using Raman
 1083 spectroscopy. *Int. J. Coal Geol.* 162, 96–107. <https://doi.org/10.1016/j.coal.2016.05.002>
- 1084 Nemčok, M., Glonti, B., Yukler, A., Marton, B., 2013. Development history of the foreland plate
 1085 trapped between two converging orogens; Kura Valley, Georgia, case study, in: Nemčok, M.,
 1086 Mora, A., Cosgrove, J.W. (Eds.), *Thick-Skin-Dominated Orogens: From Initial Inversion to*
 1087 *Full Accretion*. Geological Society, London, Special Publications 377, pp. 159–188.
 1088 <https://doi.org/10.1144/SP377.9>
- 1089 Neubauer, T.A., Harzhauser, M., Kroh, A., Georgopoulou, E., Mandic, O., 2015. A gastropod-based
 1090 biogeographic scheme for the European Neogene freshwater systems. *Earth Sci. Rev.* 143, 98–
 1091 116. <https://doi.org/10.1016/j.earscirev.2015.01.010>
- 1092 Nikishin, A.M., Wannier, M., Alekseev, A.S., Almendinger, O.A., Fokin, P.A., Gabdullin, R.R.,
 1093 Khudoley, A.K., Kopaevich, L.F., Mityukov, A. V., Petrov, E.I., Rubtsova, E. V., 2017.
 1094 Mesozoic to recent geological history of southern Crimea and the Eastern Black Sea region, in:
 1095 Sosson, M., Stephenson, R.A., Adamia, S.A. (Eds.), *Tectonic Evolution of the Eastern Black*

- 1096 Sea and Caucasus. Geological Society, London, Special Publications 428, pp. 241–264.
 1097 <https://doi.org/10.1144/SP428.1>
- 1098 Nikishin, A.M., Ziegler, P. A., Panov, D.I., Nazarevich, B.P., Brunet, M.F., Stephenson, R.A.,
 1099 Bolotov, S.N., Korotaev, M. V., Tikhomirov, P.L., 2001. Mesozoic and Cenozoic evolution of
 1100 the Scythian Platform-Black Sea-Caucasus domain, in: Ziegler, Peter A., Cavazza, W.,
 1101 Robertson, A.H.F., Crasquin-Soleau, S. (Eds.), Peri-Tethys Memoir 6: Peri-Tethyan
 1102 Rift/Wrench Basins and Passive Margins. National Museum of Natural History, Paris, pp.
 1103 295–346.
- 1104 Okay, A.I., Zattin, M., Cavazza, W., 2010. Apatite fission-track data for the Miocene Arabia-
 1105 Eurasia collision. *Geology* 38, 35–38. <https://doi.org/10.1130/G30234.1>
- 1106 Okrostsvaridze, A., Chung, S.L., Chang, Y.H., Gagnidze, N., Boichenko, G., Gogoladze, S., 2018.
 1107 Zircons U-Pb geochronology of the ore-bearing plutons of Adjara-Trialeti folded zone, Lesser
 1108 Caucasus and analysis of the magmatic processes. *Bull. Georg. Natl. Acad. Sci.* 12, 90–99.
- 1109 Pace, P., Ricciato, A., Riva, A., Tevzadze, R., Tevzadze, N., Janiashvili, A., Sanishvili, A., Alania,
 1110 V., Enukidze, O., 2019. Renewed hydrocarbon prospectivity in the Kura-Kartli Foreland
 1111 Basin, onshore Central Georgia, in: AAPG GTW Conference: Exploration and Production in
 1112 the Black Sea, Caucasus and Caspian Region, 18-19 September 2019. Batumi, Georgia, p. 20.
- 1113 Philip, H., Cisternas, A., Gvishiani, A., Gorshkov, A., 1989. The Caucasus: an actual example of
 1114 the initial stages of continental collision. *Tectonophysics* 161, 1–21.
- 1115 Pollastro, R.M., 1990. The illite/smectite geothermometer - concepts, methodology, and application
 1116 to basin history and hydrocarbon generation, in: Nuccio Vito, F., Barker Charles, E., Dyson
 1117 Sally, J. (Eds.), *Applications of Thermal Maturity Studies to Energy Exploration*. Eastwood
 1118 Print. and Publ., Denver, CO, United States, pp. 1–18.
- 1119 Pupp, M., Bechtel, A., Ćorić, S., Gratzner, R., Rustamov, J., Sachsenhofer, R.F., 2018. Eocene and

- 1120 Oligo-Miocene source rocks in the Rioni and Kura Basins of Georgia: depositional
 1121 environment and petroleum potential. *J. Pet. Geol.* 41, 367–392.
 1122 <https://doi.org/10.1111/jpg.12708>
- 1123 Qiu, N., He, L., Chang, J., Zhu, C., 2020. Research progress and challenges of thermal history
 1124 reconstruction in sedimentary basins. *Pet. Geol. Exp.* 42, 790–802.
 1125 <https://doi.org/10.11781/sysydz202005790>
- 1126 Quirico, E., Rouzaud, J.N., Bonal, L., Montagnac, G., 2005. Maturation grade of coals as revealed
 1127 by Raman spectroscopy: Progress and problems. *Spectrochim. Acta - Part A Mol. Biomol.*
 1128 *Spectrosc.* 61, 2368–2377. <https://doi.org/10.1016/j.saa.2005.02.015>
- 1129 Reilinger, R., McClusky, S., Vernant, P., Lawrence, S., Ergintav, S., Cakmak, R., Ozener, H.,
 1130 Kadirov, F., Guliev, I., Stepanyan, R., Nadariya, M., Hahubia, G., Mahmoud, S., Sakr, K.,
 1131 ArRajehi, A., Paradissis, D., Al-Aydrus, A., Prilepin, M., Guseva, T., Evren, E., Dmitrotsa, A.,
 1132 Filikov, S. V., Gomez, F., Al-Ghazzi, R., Karam, G., 2006. GPS constraints on continental
 1133 deformation in the Africa-Arabia-Eurasia continental collision zone and implications for the
 1134 dynamics of plate interactions. *J. Geophys. Res. Solid Earth* 111, 1–26.
 1135 <https://doi.org/10.1029/2005JB004051>
- 1136 Rolland, Y., 2017. Caucasus collisional history: Review of data from East Anatolia to West Iran.
 1137 *Gondwana Res.* 49, 130–146. <https://doi.org/10.1016/j.gr.2017.05.005>
- 1138 Rolland, Y., Sosson, M., Adamia, S.A., Sadradze, N., 2011. Prolonged Variscan to Alpine history
 1139 of an active Eurasian margin (Georgia, Armenia) revealed by $^{40}\text{Ar}/^{39}\text{Ar}$ dating. *Gondwana*
 1140 *Res.* 20, 798–815. <https://doi.org/10.1016/j.gr.2011.05.007>
- 1141 Sachsenhofer, R.F., Popov, S. V., Coric, S., Mayer, J., Misch, D., Morton, M.T., Pupp, M., Rauball,
 1142 J., Tari, G., 2018. Paratethyan petroleum source rocks: an overview. *J. Pet. Geol.* 41, 219–245.
 1143 <https://doi.org/10.1111/jpg.12702>

- 1144 Saintot, A., Brunet, M.-F.F., Yakovlev, F., Sébrier, M., Stephenson, R., Ershov, A., Chalot-Prat, F.,
 1145 McCann, T., 2006. The Mesozoic-Cenozoic tectonic evolution of the Greater Caucasus. *Geol.*
 1146 *Soc. Mem.* 32, 277–289. <https://doi.org/10.1144/gsl.mem.2006.032.01.16>
- 1147 Samsu, A.S., 2014. Hydrocarbon source potential of Upper Eocene and Oligo-Miocene (“Maykop”)
 1148 rocks in Georgia. MSc thesis. Montanuniversität Leoben.
- 1149 Schito, A., Andreucci, B., Aldega, L., Corrado, S., Di Paolo, L., Zattin, M., Szaniawski, R.,
 1150 Jankowski, L., Mazzoli, S., 2018. Burial and exhumation of the western border of the
 1151 Ukrainian Shield (Podolia): a multi-disciplinary approach. *Basin Res.* 30, 532–549.
 1152 <https://doi.org/10.1111/bre.12235>
- 1153 Schito, A., Corrado, S., 2018. An automatic approach for characterization of the thermal maturity of
 1154 dispersed organic matter Raman spectra at low diagenetic stages, in: Dowey, P.J., Osborne,
 1155 M., Volk, H. (Eds.), *Application of Analytical Techniques to Petroleum Systems*. Geological
 1156 Society Special Publication, pp. 107–119. <https://doi.org/10.1144/SP484.5>
- 1157 Schito, A., Corrado, S., Aldega, L., Grigo, D., 2016. Overcoming pitfalls of vitrinite reflectance
 1158 measurements in the assessment of thermal maturity: The case history of the lower Congo
 1159 basin. *Mar. Pet. Geol.* 74, 59–70. <https://doi.org/10.1016/j.marpetgeo.2016.04.002>
- 1160 Schito, A., Romano, C., Corrado, S., Grigo, D., Poe, B., 2017. Diagenetic thermal evolution of
 1161 organic matter by Raman spectroscopy. *Org. Geochem.* 106, 57–67.
 1162 <https://doi.org/10.1016/j.orggeochem.2016.12.006>
- 1163 Schito, A., Spina, A., Corrado, S., Cirilli, S., Romano, C., 2019. Comparing optical and Raman
 1164 spectroscopic investigations of phytoclasts and sporomorphs for thermal maturity assessment:
 1165 the case study of Hettangian continental facies in the Holy cross Mts. (central Poland). *Mar.*
 1166 *Pet. Geol.* 104, 331–345. <https://doi.org/10.1016/j.marpetgeo.2019.03.008>
- 1167 Shatilova, I.I., Maissuradze, L.S., Koiava, K.P., Kokolashvili, I.M., Bukhsianidze, M.G., Bruch,

- 1168 A.A., 2020. The environmental history of Georgia during the Late Miocene based of
1169 foraminifera and pollen. Universal, Tbilisi.
- 1170 Sobornov, K.O., 1996. Lateral variations in structural styles of tectonic wedging in the northeastern
1171 Caucasus, Russia. *Bull. Can. Pet. Geol.* 44, 385–399.
- 1172 Sokhadze, G., Floyd, M., Godoladze, T., King, R., Cowgill, E.S., Javakhishvili, Z., Hahubia, G.,
1173 Reilinger, R., 2018. Active convergence between the Lesser and Greater Caucasus in Georgia:
1174 Constraints on the tectonic evolution of the Lesser–Greater Caucasus continental collision.
1175 *Earth Planet. Sci. Lett.* 481, 154–161. <https://doi.org/10.1016/j.epsl.2017.10.007>
- 1176 Sosson, M., Rolland, Y., Müller, C., Danelian, T., Melkonyan, R., Kekelia, S., Adamia, S.A.,
1177 Babazadeh, V., Kangarli, T., Avagyan, A., Galoyan, G., Mosar, J., 2010. Subductions,
1178 obduction and collision in the Lesser Caucasus (Armenia, Azerbaijan, Georgia), new insights,
1179 in: Sosson, Marc, Kaymakci, N., Stephenson, R.A., Bergerat, F., Starostenko, V. (Eds.),
1180 *Sedimentary Basin Tectonics from the Black Sea and Caucasus to the Arabian Platform*.
1181 *Geological Society of London, Special Publications* 340, pp. 329–352.
1182 <https://doi.org/10.1144/SP340.14>
- 1183 Sosson, M., Stephenson, R., Sheremet, Y., Rolland, Y., Adamia, S.A., Melkonian, R., Kangarli, T.,
1184 Yegorova, T., Avagyan, A., Galoyan, G., Danelian, T., Hässig, M., Meijers, M., Müller, C.,
1185 Sahakyan, L., Sadradze, N., Alania, V., Enukidze, O., Mosar, J., 2016. The eastern Black Sea-
1186 Caucasus region during the Cretaceous: New evidence to constrain its tectonic evolution.
1187 *Comptes Rendus - Geosci.* 348, 23–32. <https://doi.org/10.1016/j.crte.2015.11.002>
- 1188 Spina, A., Vecoli, M., Riboulleau, A., Clayton, G., Cirilli, S., Di Michele, A., Marcogiuseppe, A.,
1189 Rettori, R., Sassi, P., Servais, T., Riquier, L., 2018. Application of Palynomorph Darkness
1190 Index (PDI) to assess the thermal maturity of palynomorphs: A case study from North Africa.
1191 *Int. J. Coal Geol.* 188, 64–78. <https://doi.org/10.1016/j.coal.2018.02.001>
- 1192 Su, H., Zhou, J., 2020. Timing of Arabia-Eurasia collision: Constraints from restoration of crustal-

- 1193 scale cross-sections. *J. Struct. Geol.* 135. <https://doi.org/10.1016/j.jsg.2020.104041>
- 1194 Sukhishvili, L., Forte, A.M., Merebashvili, G., Leonard, J., Whipple, K.X., Javakhishvili, Z.,
 1195 Heimsath, A., Godoladze, T., 2020. Active deformation and Plio-Pleistocene fluvial
 1196 reorganization of the western Kura fold-thrust belt, Georgia: Implications for the evolution of
 1197 the Greater Caucasus Mountains. *Geol. Mag.* <https://doi.org/10.1017/S0016756820000709>
- 1198 Tari, G., Vakhania, D., Tatishvili, G., Mikeladze, V., Gogritchiani, K., Vacharadze, S., Mayer, J.,
 1199 Sheya, C., Siedl, W., Banon, J.J.M., Sanchez, J.T., 2018. Stratigraphy, structure and petroleum
 1200 exploration play types of the Rioni Basin, Georgia, in: Simmons, M.D., Tari, G.C., Okay, A.I.
 1201 (Eds.), *Petroleum Geology of the Black Sea*. Geological Society, London, Special Publications
 1202 464, pp. 403–438. <https://doi.org/10.1144/SP464.14>
- 1203 Taylor, G.H., Teichmuller, M., Davis, A., Diessel, C.F.K., Littke, R., Robert, P., Glick, D.C.,
 1204 Smyth, M., Swaine, D.J., Vanderbroucke, M., 1998. *Organic petrology: A new handbook*
 1205 incorporating some revised parts of Stach's textbook of coal petrology. Gebruder Borntraeger
 1206 Verlagbuchhandlung.
- 1207 Tibaldi, A., Alania, V., Bonali, F.L., Enukidze, O., Tsereteli, N., Kvavadze, N., Varazanashvili, O.,
 1208 2017. Active inversion tectonics, simple shear folding and back-thrusting at Rioni Basin,
 1209 Georgia. *J. Struct. Geol.* 96, 35–53. <https://doi.org/10.1016/j.jsg.2017.01.005>
- 1210 Tibaldi, A., Bonali, F.L., Russo, E., Pasquarè Mariotto, F.A., 2018. Structural development and
 1211 stress evolution of an arcuate fold-and-thrust system, southwestern Greater Caucasus, Republic
 1212 of Georgia. *J. Asian Earth Sci.* 156, 226–245. <https://doi.org/10.1016/j.jseaes.2018.01.025>
- 1213 Tibaldi, A., Tsereteli, N., Varazanashvili, O., Babayev, G., Barth, A., Mumladze, T., Bonali, F.L.,
 1214 Russo, E., Kadirov, F., Yetirmishli, G., Kazimova, S., 2019. Active stress field and fault
 1215 kinematics of the Greater Caucasus. *J. Asian Earth Sci.* 104108.
 1216 <https://doi.org/10.1016/j.jseaes.2019.104108>

- 1217 Tissot, B.P., Pelet, R., Ungerer, P., 1987. Thermal History of Sedimentary Basins, Maturation
 1218 Indices, and Kinetics of Oil and Gas Generation. *Am. Assoc. Pet. Geol. Bull.* 71, 1445–1466.
 1219 <https://doi.org/10.1306/703c80e7-1707-11d7-8645000102c1865d>
- 1220 Tozer, R.S.J., Hertle, M., Petersen, H.I., Zinck-Jørgensen, K., 2020. Quantifying vertical
 1221 movements in fold and thrust belts: Subsidence, uplift and erosion in Kurdistan, northern Iraq,
 1222 in: Hammerstein, J.A., Di Cuia, R., Cottam, M.A., Zamora, G., Butler, R.W.. (Eds.), *Fold and*
 1223 *Thrust Belts: Structural Style, Evolution and Exploration*. Geological Society of London,
 1224 Special Publications, pp. 397–415. <https://doi.org/10.1144/SP490-2019-118>
- 1225 Vasey, D.A., Cowgill, E., Roeske, S.M., Niemi, N.A., Godoladze, T., Skhirtladze, I., Gogoladze, S.,
 1226 2020. Evolution of the Greater Caucasus basement and formation of the Main Caucasus
 1227 Thrust, Georgia. *Tectonics* 39. <https://doi.org/10.1029/2019TC005828>
- 1228 Vincent, S.J., Braham, W., Lavrishchev, V.A., Maynard, J.R., Harland, M., 2016. The formation
 1229 and inversion of the western Greater Caucasus Basin and the uplift of the western Greater
 1230 Caucasus: Implications for the wider Black Sea region. *Tectonics* 35, 2948–2962.
 1231 <https://doi.org/10.1002/2016TC004204>
- 1232 Vincent, S.J., Carter, A., Lavrishchev, V.A., Rice, S.P., Barabadze, T.G., Hovius, N., 2011. The
 1233 exhumation of the western Greater Caucasus: A thermochronometric study. *Geol. Mag.* 148,
 1234 1–21. <https://doi.org/10.1017/S0016756810000257>
- 1235 Vincent, S.J., Hyden, F., Braham, W., 2013a. Along-strike variations in the composition of
 1236 sandstones derived from the uplifting western Greater Caucasus: Causes and implications for
 1237 reservoir quality prediction in the Eastern Black Sea, in: Scott, R.A., Smyth, H.R., Morton,
 1238 A.C., Richardson, N. (Eds.), *Sediment Provenance Studies in Hydrocarbon Exploration and*
 1239 *Production*. Geological Society, London, Special Publications 386, pp. 111–127.
 1240 <https://doi.org/10.1144/SP386.15>
- 1241 Vincent, S.J., Morton, A.C., Carter, A., Gibbs, S., Barabadze, T.G., 2007. Oligocene uplift of the

- 1242 Western Greater Caucasus: An effect of initial Arabia-Eurasia collision. *Terra Nov.* 19, 160.
 1243 <https://doi.org/10.1111/j.1365-3121.2007.00731.x>
- 1244 Vincent, S.J., Morton, A.C., Hyden, F., Fanning, M., 2013b. Insights from petrography, mineralogy
 1245 and U-Pb zircon geochronology into the provenance and reservoir potential of Cenozoic
 1246 siliciclastic depositional systems supplying the northern margin of the Eastern Black Sea. *Mar.*
 1247 *Pet. Geol.* 45, 331–348. <https://doi.org/10.1016/j.marpetgeo.2013.04.002>
- 1248 Vincent, S.J., Somin, M.L., Carter, A., Vezzoli, G., Fox, M., Vautravers, B., 2020. Testing models
 1249 of Cenozoic exhumation in the Western Greater Caucasus. *Tectonics* 1–27.
 1250 <https://doi.org/10.1029/2018tc005451>
- 1251 Warr, L.N., Rice, A.H.N., 1994. Interlaboratory standardization and calibration of day mineral
 1252 crystallinity and crystallite size data. *J. Metamorphic Geol.* 12, 141–152.
- 1253 Washburn, A.M., Hudson, S.M., Selby, D., Abdullayev, N., Shiyanova, N., 2019. Constraining the
 1254 timing and depositional conditions of the Maikop Formation within the Kura Basin, Eastern
 1255 Azerbaijan, through the application of Re-Os geochronology and chemostratigraphy. *J. Pet.*
 1256 *Geol.* 42, 281–299. <https://doi.org/10.1111/jpg.12734>
- 1257 Wilkins, R.W.T., Boudou, R., Sherwood, N., Xiao, X., 2014. Thermal maturity evaluation from
 1258 inertinites by Raman spectroscopy: The “RaMM” technique. *Int. J. Coal Geol.* 128–129, 143–
 1259 152. <https://doi.org/10.1016/j.coal.2014.03.006>
- 1260 Yılmaz, A., Adamia, S.A., Chabukiani, A., Chkhotua, T., Erdoğan, K., Tuzcu, S., Karabiyikoğlu,
 1261 M., 2000. Structural correlation of the southern Transcaucasus (Georgia)-eastern Pontides
 1262 (Turkey), in: Bozkurt, E., Winchester, J.A., Piper, J.D.A. (Eds.), *Tectonics and Magmatism in*
 1263 *Turkey and the Surrounding Area*. Geological Society of London, Special Publications 173,
 1264 pp. 171–182.
- 1265 Yılmaz, A., Adamia, S.A., Yılmaz, H., 2014. Comparisons of the suture zones along a geotraverse

- 1266 from the Scythian Platform to the Arabian Platform. *Geosci. Front.* 5, 855–875.
1267 <https://doi.org/10.1016/j.gsf.2013.10.004>
- 1268 Zhou, Q., Xiao, X., Pan, L., Tian, H., 2014. The relationship between micro-Raman spectral
1269 parameters and reflectance of solid bitumen. *Int. J. Coal Geol.* 121, 19–25.
1270 <https://doi.org/10.1016/j.coal.2013.10.013>
- 1271 Zonenshain, L.P., Kuzmin, M.I., Natapov, L.M., 1990. *Geology of the USSR: A plate tectonic*
1272 *synthesis, Geodynamics Series.* American Geophysical Union, Washington, DC, United States.

Figures

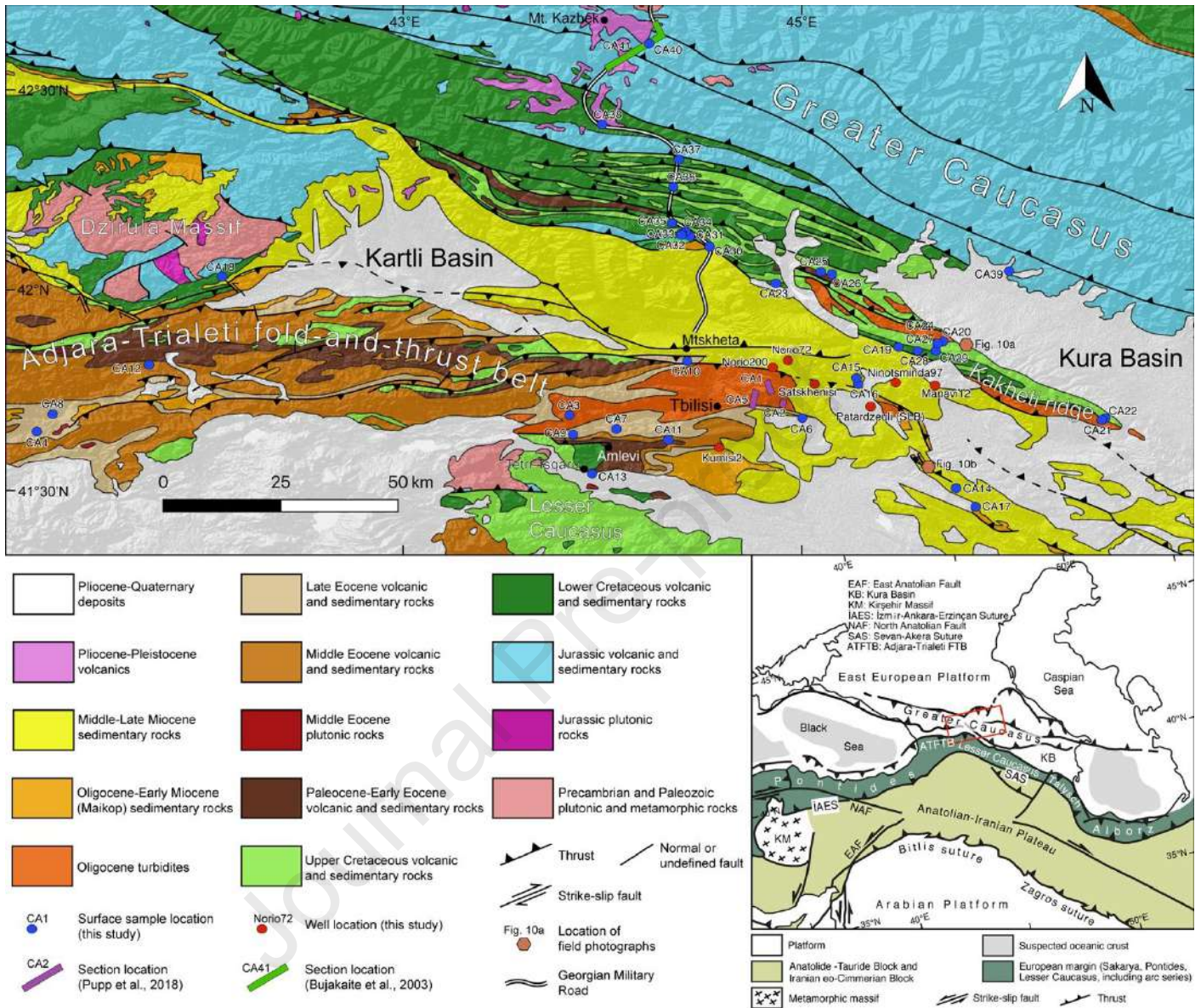


Figure 1: Geological map of the study area modified after Adamia (2004) and Gusmeo et al. (2021) with discussed sample sites and sections. Sample numbers refer to Tables 1 and 2. Locations of field photographs in Figure 10 are also shown. Lower-right inbox: geodynamic setting of the collision zone between Eurasia and Arabia (after Cavazza et al., 2019; Sosson et al., 2010). Red rectangle indicates position of Figure 3.

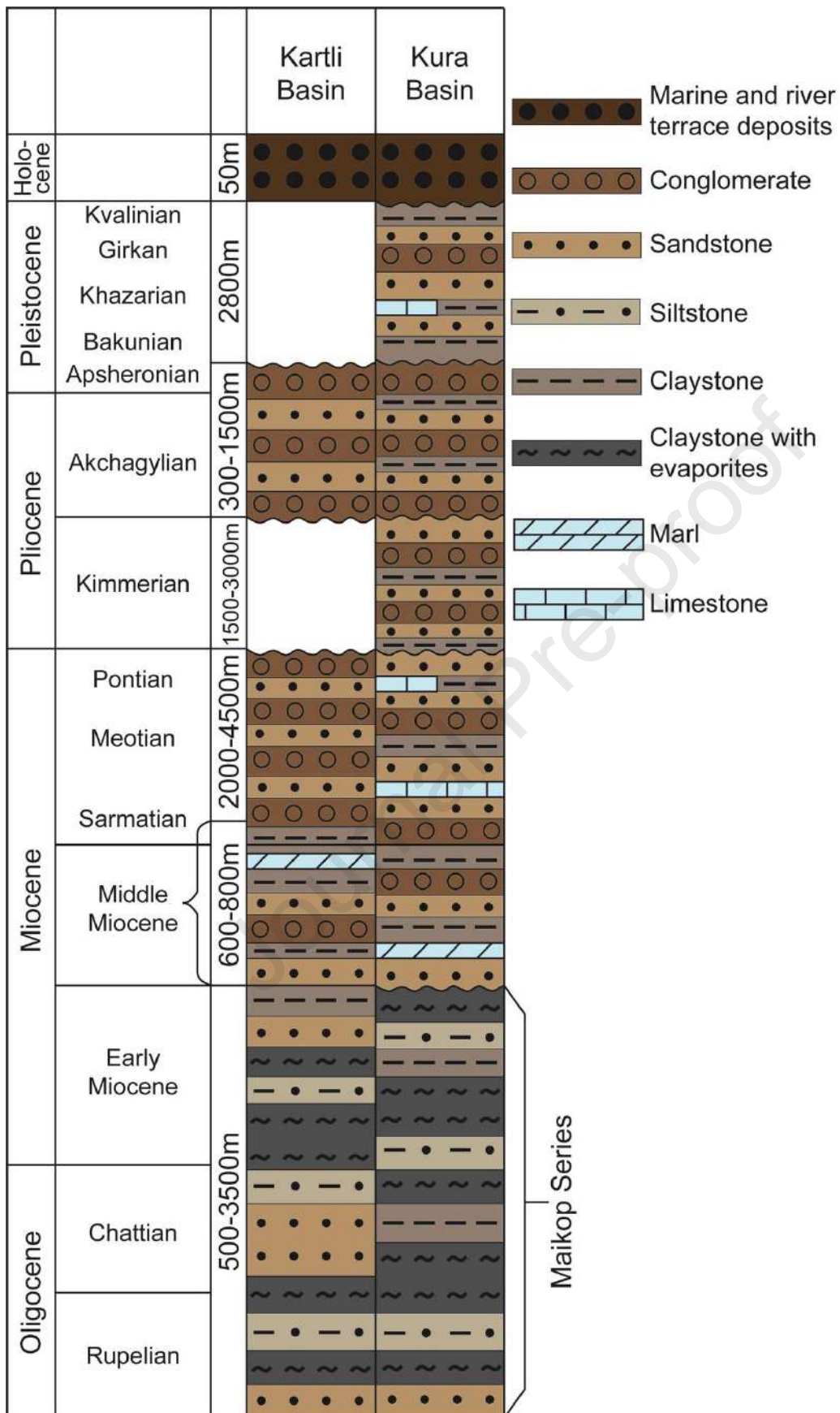


Figure 2: Schematic chrono-lithostratigraphic columns of the Kartli and Kura basins, after Adamia et al. (2010, 2011b) and Pupp et al. (2018).

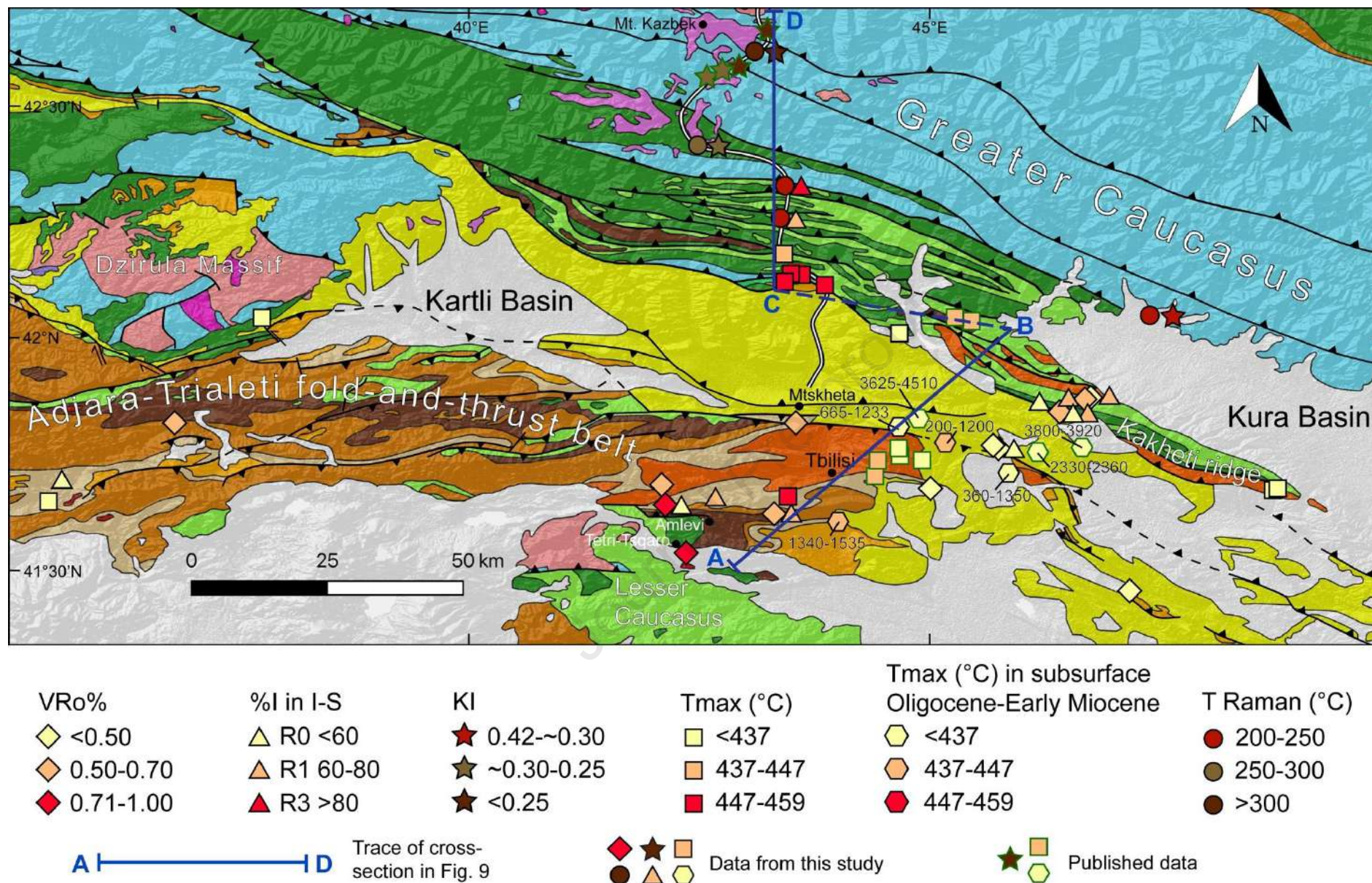


Figure 3: Geological map with original and published synthetic paleo-thermal maturity datasets. Depths of Tmax data from deep wells are shown. Base map modified after Adamia (2004) and Gusmeo et al. (2021). Colours and symbols of base map as in Figure 1.

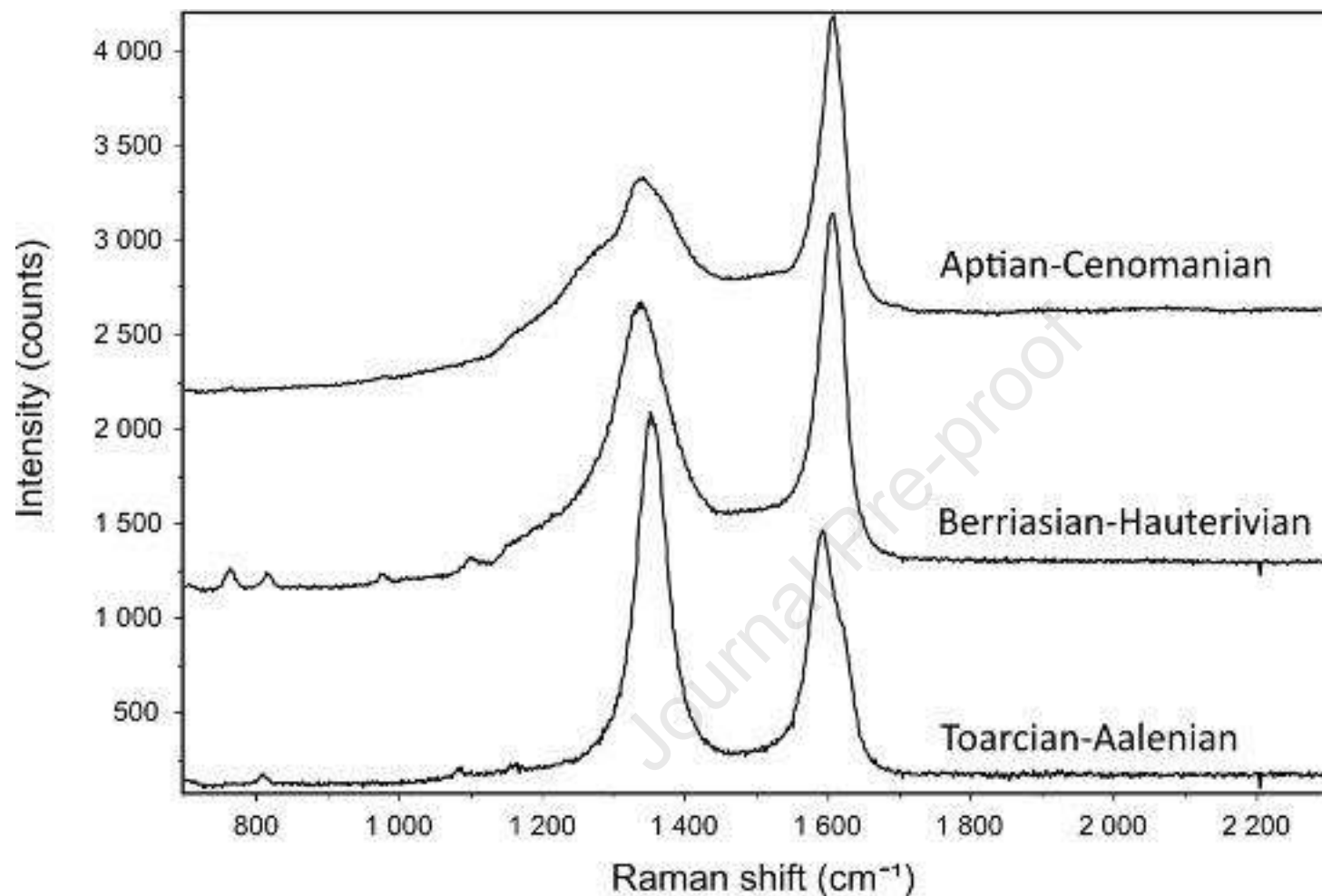


Figure 4: Selected Raman spectroscopy spectra on dispersed organic matter for samples collected across the Georgian Military Road in the Greater Caucasus. The upper spectrum refers to samples CA36 and CA37 (Aptian-Cenomanian), which are very similar, the central spectrum refers to sample CA38 (Berriasian-Hauterivian), and the lower spectrum refers to sample CA40 (Toarcian-Aalenian). D peak is around 1350 cm^{-1} and G peak is around 1600 cm^{-1} . See text for details.

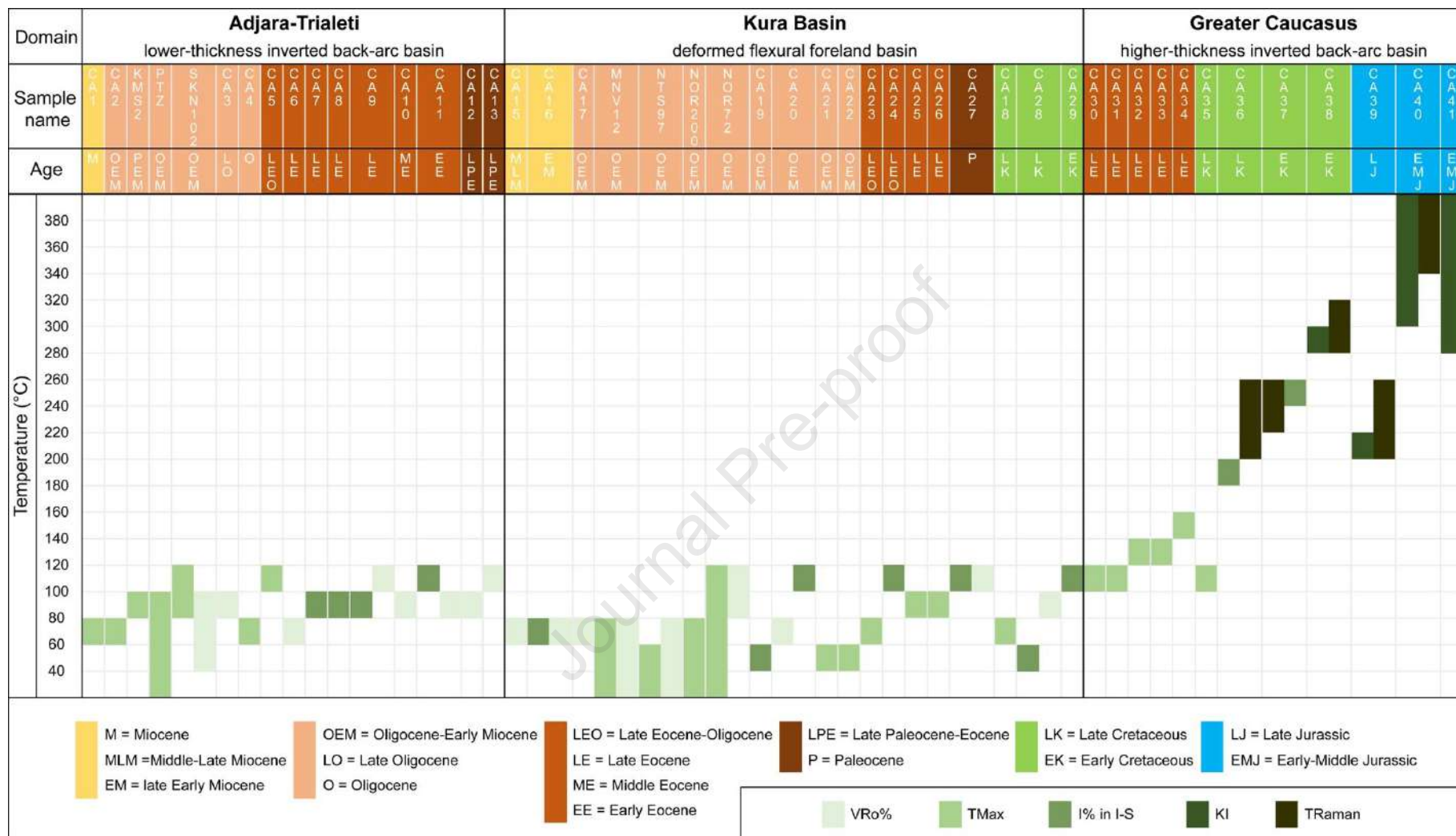


Figure 5: Correlation scheme of paleotemperatures derived from original and published samples according to VRo%, illite% and R number in illite-smectite mixed layers and Tmax with TOC >0.5%. Paleotemperatures from VRo% are derived after Barker and Pawlewicz (1986) equation; from I-S after Hoffman and Hower (1979) and from Tmax after Barnard et al., (1981). In each domain, samples are listed -from left to right- first in chronological order then in geographical (south to north) order.

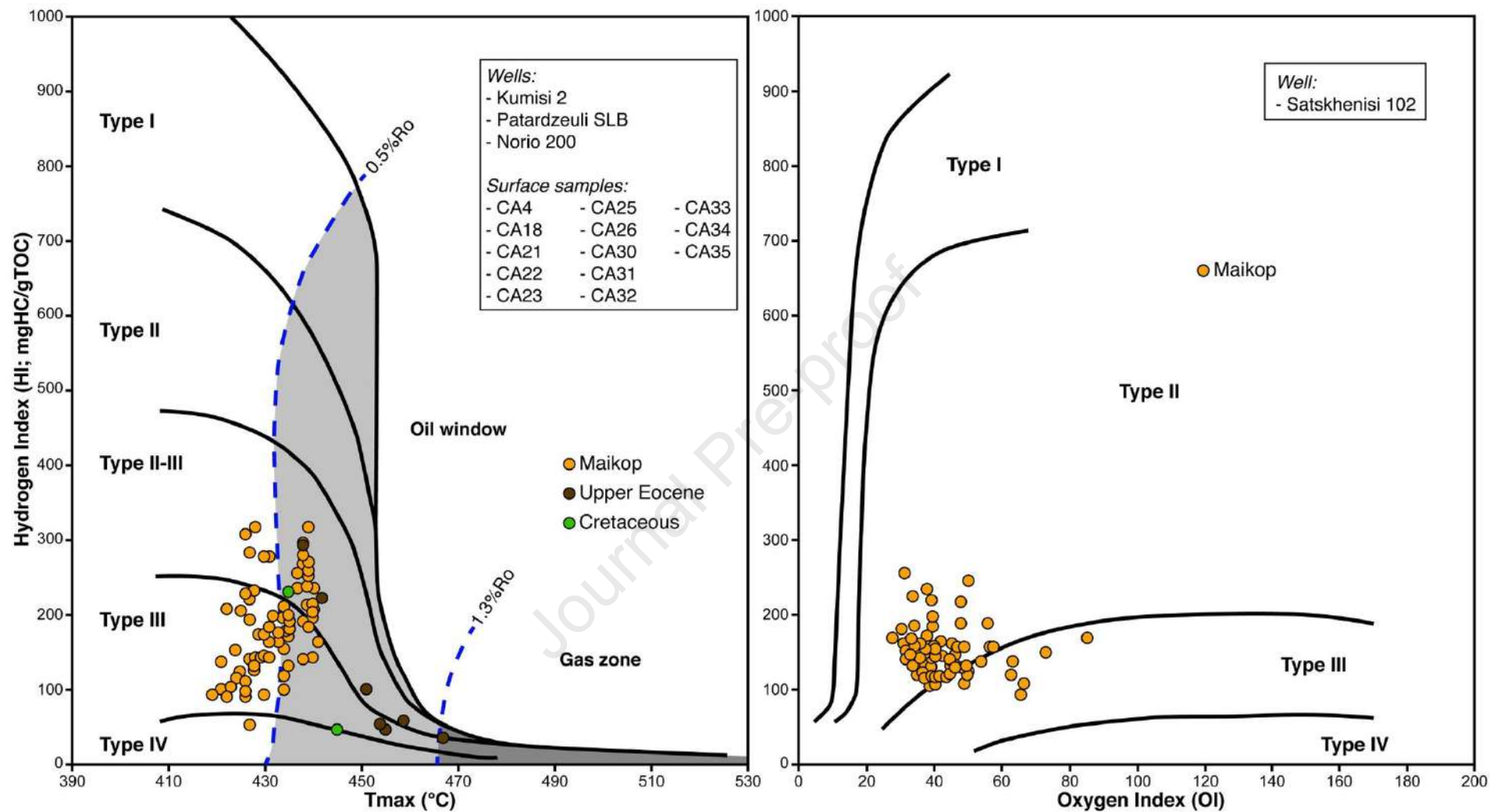


Figure 6: Tmax vs HI diagram (left) for all new data derived from wells and surface samples, subdivided according to their age, presented in this paper, except for well Satskhenisi 102 (Middle Maikop) for which a OI vs HI diagram is presented (right).

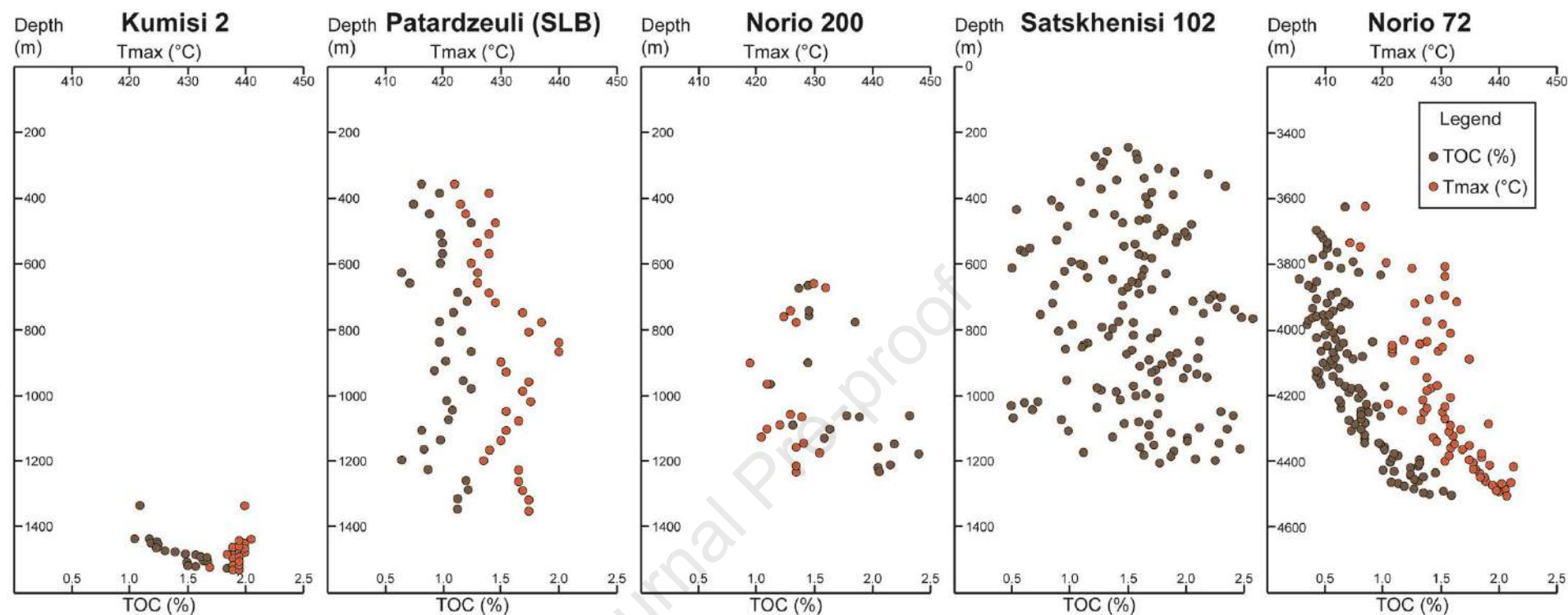


Figure 7: Depth vs Tmax (orange dots) and depth vs TOC (brown dots) plots (upper and lower x axis, respectively) for the five wells having at least two hundred metres of succession. For Satskhenisi 102 well Tmax data are not available.

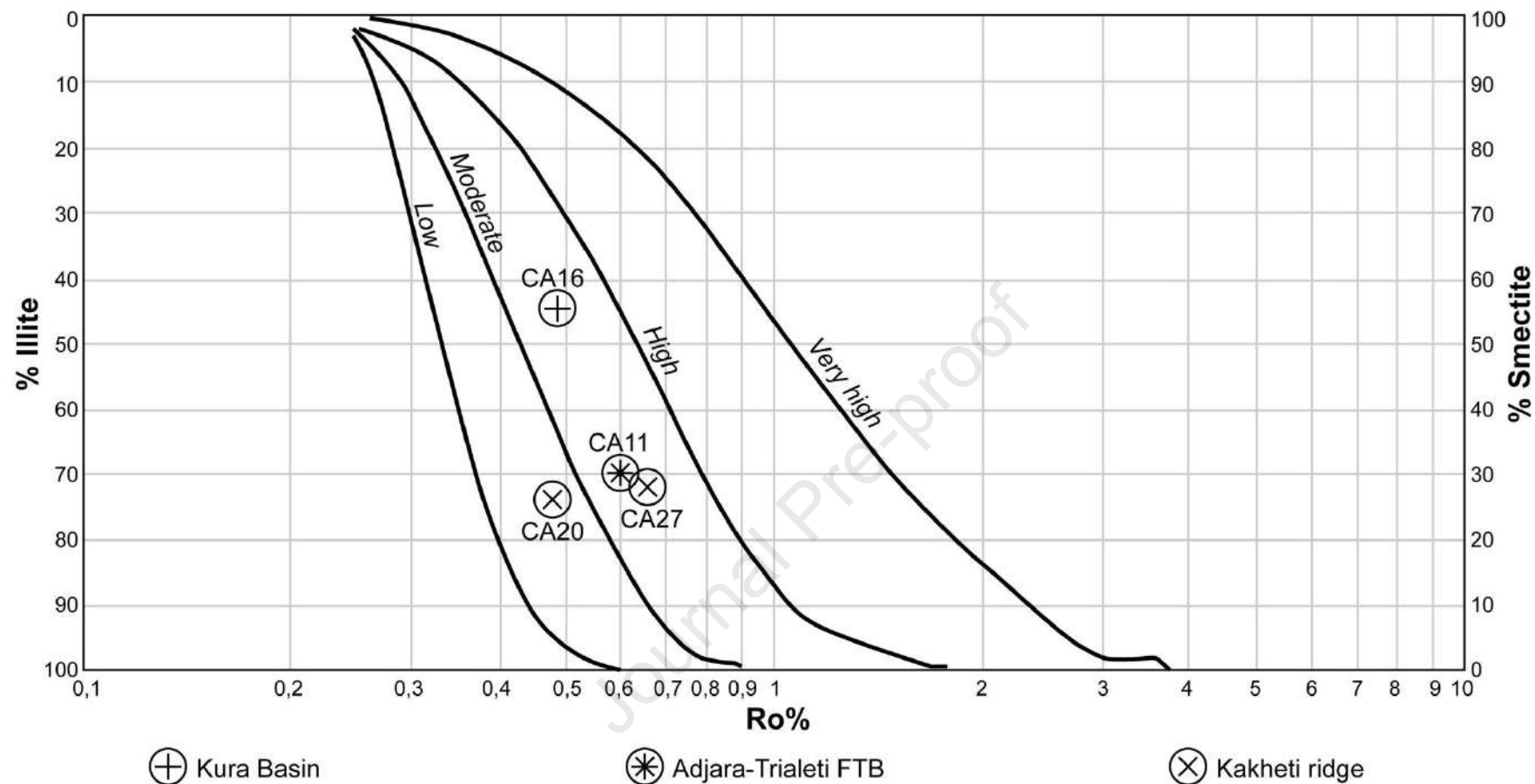


Figure 8: Correlation of VRo% (x axis) and illite% (left y axis) or smectite% (right y axis) in illite-smectite mixed layers, to derive approximate heating rates. Curves indicating heating rates are redrawn and slightly modified after Hillier et al. (1995).

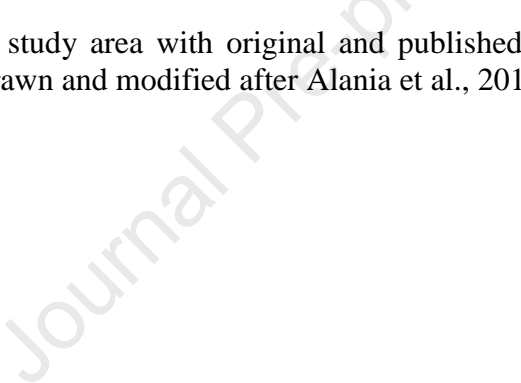




Figure 10: a) Field photograph from the northern side of the Kakheti ridge showing Pliocene-Quaternary flat-lying strata (see dotted black line) overlying Upper Cretaceous tilted rocks (yellow lines); b) Field photograph from the Kura Basin (near Rustavi town) showing tilted Oligocene (Maikop) sandstones and siltstones unconformably overlain (yellow dotted line) by flat-lying Late Pliocene-Early Pleistocene conglomerates. Both images demonstrate that the main phase of deformation within the Kura Basin/Kakheti ridge ended before the Late Pliocene, but uplift continued without tilting. Locations are indicated in Figure 1.

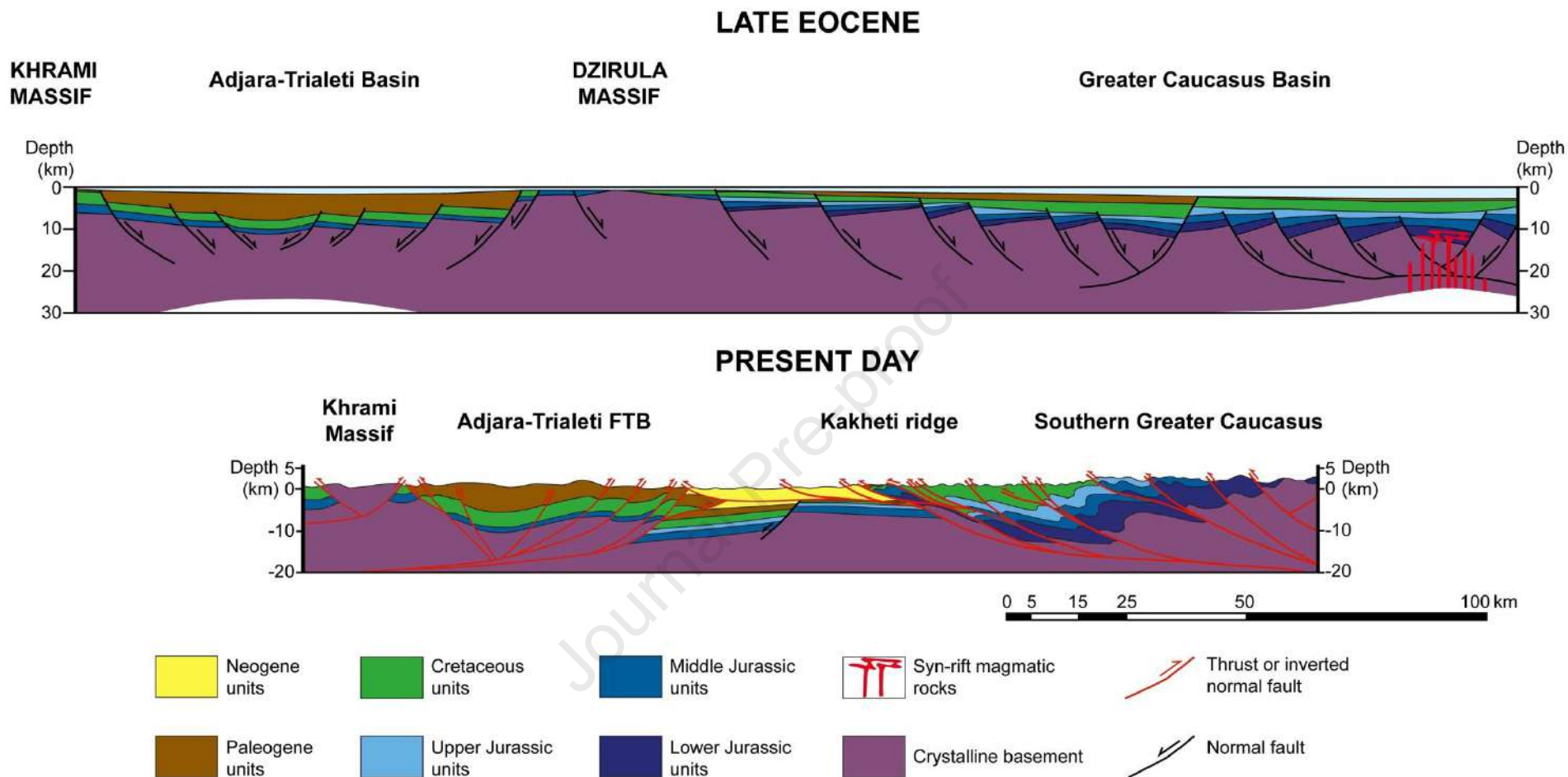


Figure 11: Schematic cartoon of the structural-stratigraphic setting of the study area across the Dzirula Massif, extending to the south in the Adjara-Trialeti FTB, derived from inversion of a Cenozoic back-arc basin, and to the north across the Greater Caucasus, derived from inversion of a Mesozoic rift basin. Redrawn and modified after Alania et al., 2017; Gusmeo et al., 2021; Mauvilly et al., 2016.

Table 1

Thermal maturity data derived from surface samples.

Sample name	Geological domain	Coordinates	Age	Ro% ± sd (measured fragments)	Tmax (with TOC >0.5) (°C)	Hydrogen Index (mgHC/gTOC)	T Raman (°C) ± sd (n° measurements)	XRD <2µm composition	I% in I-S (R Nr)	Kubler Index	Reference
CA1	Adjara-Trialeti FTB	-	Miocene	-	<437	-	-	-	-	-	Pupp et al., 2018
CA2	Adjara-Trialeti FTB	-	Late Oligocene-Miocene	-	429-435	-	-	-	-	-	Pupp et al., 2018
CA3	Adjara-Trialeti FTB	38N 0452009 4616299	Late Oligocene	0.51 ± 0.04 (36)	-	-	-	-	-	-	This study
CA4	Adjara-Trialeti FTB	38N 0325498 4610679	Oligocene	-	430	93	-	-	-	-	This study
CA5	Adjara-Trialeti FTB	-	Late Eocene-Oligocene	-	446-448	-	-	-	-	-	Pupp et al., 2018
CA6	Adjara-Trialeti FTB	38N 0500906 4615010	Late Eocene	0.47 ± 0.03 (33)	-	-	-	-	-	-	This study
CA7	Adjara-Trialeti FTB	38N 0461429 4612640	Late Eocene	-	-	-	-	I ₃₃ I-S ₄₀ C-S ₂₈	76 (R1)	-	This study
CA8	Adjara-Trialeti FTB	38N 0343226 4618483	Late Eocene	-	-	-	-	I ₄₅ I-S ₂₄ Ch ₃₁	32 (R0)	-	This study
CA9	Adjara-Trialeti FTB	38N 0452684 4611098	early Late Eocene	0.74 ± 0.04 (48)	-	-	-	I ₅ I-S ₂₅ C-S ₃₉ Ch ₃₀	27 (R0)	-	This study
CA10	Adjara-Trialeti FTB	38N 0476497 4631400	Middle Eocene	0.50 ± 0.05 (19)	-	-	-	I ₆ C-S ₆₇ Ch ₂₈	-	-	This study
CA11	Adjara-Trialeti FTB	38N 0472357 4609370	Early Eocene	0.60 ± 0.05 (21)	-	-	-	I ₃₀ I-S ₂₄ C-S ₁₆ Ch ₃₀	70 (R1)	-	This study
CA12	Adjara-Trialeti FTB	38N 0363775 4631968	Late Paleocene-Early Eocene	0.60 ± 0.04 (23)	-	-	-	I ₇₂ C-S ₂₂ Ch ₆	-	-	This study
CA13	Adjara-Trialeti FTB	38N 0456357 4599540	latest Paleocene-Early Eocene	0.77 ± 0.06 (41)	-	-	-	I ₁₇ C-S ₅₀ Ch ₃₃	-	-	This study
CA14	Kura Basin	38N 0500909 4595159	Late Miocene	-	-	-	-	Sm ₈₅ I ₁₀ Ch ₅	-	-	This study
CA15	Kura Basin	38N 0512307 4625099	Middle-Late Miocene	0.43 ± 0.05 (92)	-	-	-	-	-	-	This study
CA16	Kura Basin	38N 0512536 4624356	late Early Miocene	0.49 ± 0.05 (23)	-	-	-	I ₄₇ I-S ₁₉ K ₃₂ Ch ₂	45 (R0)	-	This study
CA17	Kura Basin	38N 0537395 4591009	Oligocene-Early Miocene	0.40 ± 0.03 (31)	-	-	-	-	-	-	This study
CA18	Dzirula Massif/Kura	38N 0379736 4652510	Cretaceous	-	<437	230	-	-	-	-	This study
CA19	Kakheti Ridge	38N 0520846 4635330	Oligocene-Early Miocene	-	-	-	-	I ₅₄ I-S ₂₆ K ₁₀ Ch ₁₀	15 (R0)	-	This study
CA20	Kakheti Ridge	38N 0529855 4636895	Oligocene-Early Miocene	0.48 ± 0.03 (46)	-	-	-	I ₆₄ I-S ₂₄ K ₁₀ Ch ₂	74 (R1)	-	This study
CA21	Kakheti Ridge	38N 0563536 4615033	Oligocene-Early Miocene	-	427	51	-	-	-	-	This study
CA22	Kakheti Ridge	38N 0563937 4615428	Oligocene-Early Miocene	-	421	99	-	-	-	-	This study
CA23	Kakheti Ridge	38N 0495174 4652984	Late Eocene-Oligocene	-	434	99	-	-	-	-	This study
CA24	Kakheti Ridge	38N 0529177 4636408	Late Eocene-Oligocene	-	-	-	-	I ₅₃ I-S ₂₁ K ₁₅ Ch ₁₂	72 (R1)	-	This study
CA25	Kakheti Ridge	38N 0505210 4652984	Bartonian-Lower Priabonian	-	438	292	-	-	-	-	This study
CA26	Kakheti Ridge	38N 0506810 4656464	Late Eocene	-	442	222	-	-	-	-	This study
CA27	Kakheti Ridge	38N 0529177 4636408	Paleocene	0.66 ± 0.05 (7)	-	-	-	I ₆₄ I-S ₂₄ K ₁₀ Ch ₂	72 (R1)	-	This study
CA28	Kakheti Ridge	38N 0524721 4634599	Maastrichtian	0.63 ± 0.06 (40)	-	-	-	I ₁₄ I-S ₈₆	18 (R0)	-	This study
CA29	Kakheti Ridge	38N 0528762 4634818	Hauterivian-Albian	-	-	-	-	I ₃₂ I-S ₉ K ₂₈ Ch ₃₁	75 (R1)	-	This study
CA30	Greater Caucasus	38N 0481457 4663658	Late Eocene	-	454	53	-	-	-	-	This study
CA31	Greater Caucasus	38N 0476888 4666996	Late Eocene	-	451	101	-	-	-	-	This study
CA32	Greater Caucasus	38N 0475448 4667103	Late Eocene	-	459	57	-	-	-	-	This study
CA33	Greater Caucasus	38N 0475448 4667135	Late Eocene	-	455	46	-	-	-	-	This study
CA34	Greater Caucasus	38N 0476401 4667399	Late Eocene	-	467	36	-	-	-	-	This study
CA35	Greater Caucasus	38N 0472854 4669914	Cenomanian	-	445	45	-	-	-	-	This study
CA36	Greater Caucasus	38N 0473963 4680238	Cenomanian	-	-	-	216 ± 13 (7)	I ₁ I-S ₂₈ Ch ₇₁	80 (R3)	-	This study
CA37	Greater Caucasus	38N 0474870 4688016	Aptian-Albian	-	-	-	228 ± 5 (14)	I ₈₇ I-S ₈ Ch ₅	88 (R3)	-	This study
CA38	Greater Caucasus	38N 0459110 4697896	Berriasian-Hauterivian	-	-	-	292 ± 7 (17)	I ₈₈ C-S ₁ Ch ₁₁	86 (R3)	0.29	This study
CA39	Greater Caucasus	38N 0544064 4656874	Oxfordian-Tithonian	-	-	-	235 ± 22 (16)	I ₈₂ C-S ₁₂ Ch ₆	-	0.43	This study
CA40	Greater Caucasus	38N 0469216 4720975	Toarcian-Aalenian	-	-	-	379 ± 9 (15)	I ₄₆ Ch ₅₄	-	0.10	This study
CA41	Greater Caucasus	-	Lower-Middle Jurassic	-	-	-	-	-	-	<0.30	Bujakaite et al., 2003

List of surface original and published data analysed and discussed in the paper with samples name, geological domain, location, age, selected paleo-thermal parameters (VRo%, Tmax with TOC>0.5, HI, TRaman, I% in I-S, KI) and <2 µm XRD composition. Original and published data are indicated from south to north. Pyrolysis data are derived using various editions of IFP Rock-Eval technology (see Behar et al. (2001) and references therein). For <2 µm XRD composition: Ch = Chlorite, C-S = Chlorite-Smectite mixed layers, I = Illite, I-S = Illite-Smectite mixed layers; K = Kaolinite, Sm = Smectite.

Table 2

Thermal maturity data derived from wells.

Well	UTM Coordinates	Age	Geological domain	Analysed depth (top-bottom, m)	Analysed thickness (m)	Mean Tmax (°C) (Min, Max)	Mean TOC (Min, Max)	Mean HI (Min, Max)	Nr samples	Sample type	Average Ro%	Reference
Kumisi 2	38N 0483141 4607313	Oligocene-Early Miocene	Adjara-Trialeti FTB	1340-1535	195	439 (434, 441)	1.44 (1.05, 1.95)	222 (117-318)	21	cuttings	-	This study
Patardzeuli (SLB)	38N 0515117 4618697	Oligocene-Early Miocene	Adjara-Trialeti FTB	360-1350	990	431 (422, 440)	1.01 (0.64, 1.25)	155 (91-235)	34	cuttings	-	This study
Satskhenisi 102	38N 0507754 4625925	middle Maikop, Late Oligocene	Adjara-Trialeti FTB	200-1200	1000	(437-447)	(0.50, 2.40)	(91-259)	148	cuttings	0.3-0.6	This study
Norio 200	38N 0494735 4629461	Oligocene	Kura Basin	665-1233	568	426 (419-432)	1.77 (1.13, 2.41)	223 (90-318)	18	cuttings	<0.5	This study
Norio 72	38N 0500117 4630132	Oligocene	Kura Basin	3625-4510	885	429 (415-442)	0.80 (0.30, 1.61)	128 (77-208)	64	cuttings	0.5-0.7	Samsu, 2014
Ninotsminda 97	38N 0524029 4624730	lower Maikop, Early Oligocene	Kura Basin	2330-2360	30	422 (421-424)	0.76 (0.63, 0.82)	100 (98-102)	4	cuttings	<0.5	Samsu, 2014
Manavi 12	38N 0535573 4623781	Oligocene-Early Miocene	Kura Basin	3800-3920	120	424 (407-431)	4.20 (3.30, 5.40)	200 (120-279)	32	cuttings	<0.5	Samsu, 2014

List of wells used in this study, with wells name, location, age, thickness and depth of the section considered, Tmax, TOC, HI and VRo% data. Pyrolysis data are derived using various editions of IFP Rock-Eval technology (see Behar et al. (2001) and references therein).

Highlights

- *New multi-proxy thermal maturity dataset from Adjara-Trialeti to Greater Caucasus*
- *Thermal maturity jump from Greater Caucasus to Adjara-Trialeti FTB and Kura Basin*
- *Positive inversion of rift basins into Adjara-Trialeti FTB and Greater Caucasus*
- *Thin-skinned deformation in Kura Basin/Kakheti above pre-shortening structural high*

Declaration of interests

☒ The authors declare that they have no known competing financial interests or personal relationships that could have appeared to influence the work reported in this paper.

☐ The authors declare the following financial interests/personal relationships which may be considered as potential competing interests:

--